INTEGRATED REGIONAL ENSTROPHY AND ITS CORRELATION WITH REGIME TRANSITIONS IN THE NORTHERN HEMISPHERE

A Thesis Presented to the Faculty of the Graduate School at the University of Missouri

In Partial Fulfillment of the Requirements for the Degree Masters of Science

By

EMILY M. KLAUS

Dr. Anthony Lupo, Thesis Advisor

MAY 2019

The undersigned, appointed by the dean of the Graduate School, have examined the thesis entitled

INTEGRATED REGIONAL ENSTROPHY AND ITS CORRELATION WITH REGIME TRANSITIONS IN THE NORTHERN HEMISPHERE

Presented by Emily M. Klaus,

a candidate for the degree of master of science,

and hereby certify that, in their opinion, is worthy of acceptance.

Professor Anthony Lupo

Professor Patrick Market

Associate Professor Mark Palmer

Acknowledgements

First, I would like to extend my sincerest gratitude to my thesis committee, Dr. Patrick Market, Dr. Mark Palmer, and especially to my thesis committee chair and advisor, Dr. Anthony Lupo. I couldn't be more grateful and appreciative of your patience and guidance. A large thank you goes out to the Missouri Student Unions for funding my education here at the University of Missouri. Another thank you goes out to Dr. Fox and Eric Aldrich, and again to Dr. Market and Dr. Lupo for all your guidance and expertise in my six years here. I honestly could not have asked for a better set of professors to teach the coursework, and to have the patience to deal my questions and difficulties. Another thank you goes out to my fellow graduate students. You are were a fantastic community to fall back on when I had questions or needed help, or when a much needed break was due.

Next, I want to thank my family and friends outside of the department for all of the support and encouragement that kept me going. Thanks goes out specifically out to my Unions family for being a haven for me to escape from the depths of the grad office, and for being a place for me to learn and develop. The friendships and connections I have made through the Unions will forever be treasured. Moreover, a massive thanks goes out to my family here in Columbia and Farmington, Missouri. None of this would have been possible if I didn't have you all there to help me get through. Lastly, and most importantly, I would like to thank my Lord and Savior for providing me with this opportunity and privilege to continue my education. Nothing of this would have been possible if He didn't have my back. "*Trust in the Lord with all your heart, and lean not on your own understand. In all your ways, acknowledge Him, and He will make your paths straight.*" – Proverbs 3:5-6

Table of Contents

List of Figures

List of Tables

Abstract

Integrated regional enstrophy (IRE) is the enstrophy integrated over a portion of the globe at a specific level in the atmosphere. Previous work has shown this quantity is correlated to the positive Lyapunov Exponent for hemispheric flow, and as such is a measure of flow stability or predictability. In this study, IRE is calculated at 500-hPa over an area that encompasses 0° to 70° N in the Northern Hemisphere. The data sets used were the 500-hPa initial and forecast fields for the Global Ensemble Forecasting System (GEFS) (on a 1° x 1° latitude-longitude grid) provided by the National Oceanic and Atmospheric Administration (NOAA) Weather Prediction Center (WPC) and the National Centers for Environmental Prediction / NOAA reanalysis (on a 2.5° x 2.5° latitude-longitude grid) archived in Boulder, CO. The GEFS forecast fields were provided every 24-h out to 240-h. By examining these forecasts over a year, we have found that significant changes in IRE values are a good predictor of flow regime transition, and several cases were found. We also found that the IRE forecasts identified these regime transitions reliably out to four days, and the skill decreased significantly after this time. Additionally, a threshold for changes in IRE was found for the cases studied here and this threshold varied by season.

Chapter 1: Introduction

Earth's atmosphere is a turbulent, ever-changing system that can be difficult to forecast [1]. Past research has examined planetary-scale flow patterns, also referred to as large-scale flow regimes, and their tendency to reoccur and/or persist in certain regions of the Northern Hemisphere (NH). In this study, the planetary-scale refers to flows with time scales of 7-14 days of 6000-km or more. Small-scale in this study refers to synoptic-scale flows with time scales of 1-7 days of 1,500-km - 6000-km. Both scales are corrected by inertial forces. On the planetary scale in the NH, flow patterns, such as blocking, have been found to have correlations between areas over the North Pacific and the Eastern US [2-5]. These large-scale correlations are called teleconnections [5]. Knowing when these patterns occur and how they affect certain regions is applicable in long-range forecasting [39][40]. When generating forecasts for ten days or more, these phenomena are helpful to explain the dynamics involved in long-range forecasting methods, such as: analog, climatology, dynamics, numerical, persistence, and statistical. Having additional methodology or tools to forecast regime transition would continue to improve our predictions for short or long-range forecasts. However, predictability is limited by an incomplete representation or even a full understanding of relevant physical processes in the atmosphere [6].

In order to enhance our projections of how large-scale flow will progress and change (e.g. flow regime transition or change), generating a numerical weather prediction method to forecast or identify regime transitions would be useful. In [7], they state that forecasters rely on numerical models to make synoptic scale predictions, which can be made out to seven days with the forecasting limit sitting at 10-14 days. In recent studies, it has been

shown that integrated regional enstrophy, also referred to as IRE, can be used as a measure for identifying, in general, the transition of large-scale flows [8-12]. IRE can also indicate blocking onset or decay and had been found to be a flow instability indicator [8-12]. It was suggested in [2] [10] and [13], that blocking regimes will decay when there is a large enough change in large-scale flow regimes. Although [14] [15] demonstrates that blocking can survive flow regime transition if the synoptic-scale dynamics are favorable.

Blocking can be defined as a dynamic ridging in the jet stream or as stated by [16] is a persistent large-scale mid-latitude positive geopotential height anomaly. Blocking is driven by the phasing between the synoptic-scale storm tracks with a large-scale quasi-stationary ridge [17][18] [19]. It is important to note that blocking is driven in part by large-scale flow patterns, but not the general circulation. Jensen [8] along with [10] and [13] suggests that blocking does not survive regime transition. In the NH, blocking involves strong planetary-scale and synoptic-scale interactions [17] [20] [21] [22] [23] [24] [25] [26] while the Southern Hemisphere blocking results from the superposition between the two scales [18]**.** The decay of blocking is a more complex problem involving synoptic and planetary-scale interactions than block onset or maintenance [3] [10], which is why blocking is not a one-to-one indicator of flow regime transition. Therefore, blocking can create forecasting challenges for projecting regional weather patterns out to ten days [27].

Past research continues to point in the direction of IRE as being a useful tool in indicating blocking onset/decay, but this can also be a useful tool in projecting regime transition [28]. For example, in [10] [11] they found IRE to be a reliable indicator of blocking onset and decays by showing local maxima in the IRE values. In [20] and [8], it is noted that IRE increased locally with the decay studied blocking events, and also that

IRE values were comparatively low during maintenance periods. Additionally, studies found that IRE could identify flow regime transitions overall, even if blocking was present or not [8] [12] [29].

1.1 Purpose and Objectives

Since research suggests that not only is IRE a good indicator of blocking onset/decay and regime transitions, even if blocking is not present IRE is still a reliable method for projecting regime transitions exclusively. This is the main purpose of this research, to demonstrate that IRE is a good indicator of regime transitions through the use of case studies and ensemble model forecasts during the months of August 2018 through February 2019. The case studies used in this research were analyzed in order to test IRE skill, and whether or not this is a useful operational indicator of regime transitions. In performing this research, a threshold for IRE change with time during regime transition will be identified as well as an examination of how much lead-time an ensemble model forecast system can provide for these transitions. Section two will list the data sets used in this research including the ensemble modeling system. The methodology is also outlined in section two, as well as a description of the selection of our events in order to test IRE forecasting skill. The measures for skill will be based on the forecast verification methods used in [30]. Section three will describe and analyze the cases and section four will summarize the findings of this research and present the conclusions.

Chapter 2: Methodology

2.1 Data

For this research, 500-hPa height data (m) at 1200 UTC daily for the months of February 2018 through February 2019. These images are provided by the National Centers for Environmental Prediction/National Center for Atmospheric Research (NCEP/NCAR) re-analysis which provide large-scale meteorological data on 2.5° × 2.5° latitude-longitude grids [31]. These images are archived at NCAR's research facility in Boulder, CO. Northern Hemisphere daily 500-hPa anomaly maps for the months of August 2018 through February 2019 were also used for verification in this research [32]. This research also examined Hovemoller diagrams based on the NCEP 500-hPa reanalysis. These datasets were averaged over the 5° latitude band centered on 40°N and are provided from the Climate Prediction Center's Climate Diagnostic Bulletin for each respective month. For this research, the images from August 2018 through February 2019 were used.

NCEP's Global Ensemble Forecast System (GEFS) uses the NCEP Global Forecast System (GFS) model for integration and breeding technique to generate perturbations in the initial conditions [33]. NCEP North American Ensemble Forecast System (NAEFS) is one of GEFS's many forecast projects, where IRE data is provided by NAEFS. Within the NAEFS, ensemble producing centers exchange their raw forecast data, they statistically post-process (include down-scaling) all ensemble members, and jointly [with other members] develop and produce end products based on the combined ensemble of forecasts [33]. The NAEFS combines the Canadian global forecast model ensemble and the National Weather Service global forecast model ensemble into a joint ensemble that creates

weather forecasts for North America [34]. When combined, the ensemble can provide weather forecast guidance for the 1-14 day period with a 1° x 1° resolution that is of higher quality than the currently available operational guidance based on either set of ensembles alone [35].

2.2 Methods

Dymnikov et al. [9] demonstrated that over the Northern Hemisphere (NH), the (sum of) the positive Lyapunov Exponent(s) for the flow is strongly correlated with the NH area integrated enstrophy (IE). Lyapunov exponents can be defined as the average rate of exponential divergence or convergence of nearby trajectories, and can be used as a test for chaos in a system or provides a quantitative measurement of Sensitive Dependence on Initial Conditions (or SDOIC). Lyapunov exponents can also represent the predictability and stability properties of a dynamical system without the need to explicitly solve for the flow streamfunction [11].

IRE, also known as integrated regional enstrophy, is the square of relative vorticity integrated over an area [0° to 70° N] in this case

$$\text{IRE} = \sum_{i>0} \lambda_i \approx \int_A \zeta^2 dA \quad (1)$$

where λ_i is the ith Lyapunov exponent that is greater than zero in a dynamic system, ζ is the vorticity (the curl of the wind vector), where the amount squared is called enstrophy (which is the dissipation tendency of a fluid), [8]. In (1), vorticity is calculated at 500-hPa with the geostrophic relationship using a second order finite differencing. Athar and Lupo [11] demonstrated that sufficiently large areas of the NH flow will have IRE values that correlate highly to those calculated over the entire NH. Here, enstrophy is integrated over most of the NH [0° to 70° N].

Lyapunov exponents can have positive or negative values in an n-dimensional system. Positive values indicate that trajectories within a phase space or manifold separate at an exponential rate, whereas a negative value infers convergence as time goes to infinity. When taking the sum of the positive Lyapunov exponents, a larger value represents faster divergence, so less predictability can be assumed. Thus, the same principle relates to IRE [8] [31]. A smaller IRE indicates the atmospheric flow is relatively stable, and we can assume models will behave in a predictable fashion. Conversely, when the IRE is larger, we can expect more unstable flow or less predictability.

The research conducted in [28] and [11] demonstrate that IRE could be used as an indicator of the onset or termination of blocking. The onset and termination of blocking were identified by looking for local maxima in a time series of IRE. However, Jensen and Lupo [28] and subsequent publications [2] showed that local maxima in IRE can occur independently of blocking and used to identify the transition of NH flow regimes from one state to another. Jensen et al. [2] used IRE to identify these flow regime transitions in near-term climate model simulations and compared this to the climatological frequency of these transitions during the most recent period. Thus, in this study, it is proposed that IRE can be used as a diagnostic tool for identifying flow regime transitions in an operational environment.

As stated above, we can assume that the area between 0° latitude and 70° N is a large fraction of the NH for the purposes of calculating IRE. Here, IRE values are calculated for the initial GEFS model field of 1° x 1°, and then in the forecast fields every 24 hours up to 240 hours. This would represent forecasts for days 1-10. We can assume a greater divergence in the solutions from observed IRE value when comparing the 24-hour

forecast with the 240-hour forecast. IRE values in this dataset typically range from 0.60 $km^2 \cdot s^{-2}$ through 0.85 $km^2 \cdot s^{-2}$, whereas it had been found that local maxima of IRE correspond to transitioning large-scale flows with lesser predictability [8] [7] [28].

Using the procedure from [30] on testing forecast skill, in this study, Day 1, 4, 7, and 10 were used in testing the forecast skill of IRE and are also used to demonstrate how extended forecast solutions diverged from the observed IRE with time. The method described in [30] is typically used for mesoscale and synoptic events (e.g. severe weather). Research in [30] showed that their results in testing the skill of the Bering Sea Rule and the East Asia Rule for 7-11 and 17-22 day periods were consistent with climatology. Therefore, the methods used in [30] are applicable in studies such as this.

As used in [30], this methodology allows for the scoring of forecast Days 1, 4, 7, and 10 versus the corresponding observed IRE value. Renken et al. [30] tested their skill with the following equation

$$\text{Skill}=\frac{(Forecast-Base)}{(Verification-Base)} \tag{2}$$

where "Forecast" is the projected value, "Verification" is the observed value, and "Base" is a baseline forecast, usually a climatological value that relates to the skill testing. Since we did not have a base to use in our study due to lack of climatological record of IRE, we used (2) to design our own skill test, as seen below in (4).

The procedure used in [30] uses signal detection theory, which is borrowed from the National Weather Service and others, and typically used in the forecasting of smaller scale events such as severe weather. In signal detection theory (Table 1), the variables X, Y, Z, and W are used in a two by two box to determine if the event was observed and forecast (X or HIT), if the event was observed but not forecast (Y or MISS), if the event was not

observed but forecast (Z or FALSE ALARM), and if the event was no observed and not forecast (W or NULL), respectively. This procedure will be used to determine how IRE behaved with specific events, and is shown below.

Observed (below)/Forecast (right)	Yes	No
Yes	X	Y
No	Z	W

Table 1: Contingency table for (Renken et al., 2017) Signal Detection Theory.

In order to determine whether the IRE forecasts produce signal above the background noise, the sensitivity index (d) is used (references). The sensitivity index is calculated as:

$$D = z(POD) - z(FAR) \quad (3)$$

Where z(POD) and z(FAR) are the statistical z-score test values that correspond to POD and FAR. This will result in a measure of statistical significance [41][42].

2.3 Defining IRE Thresholds

In order to demonstrate our procedure, first the absolute value of the difference between the observed IRE and the Day 1 model IRE (and the observed IRE and the Days 4,7, and 10 model IRE) was calculated for the months of August 2018 through February 2019, as shown in Figures 1-4, in order to identify how model IRE differed from the observed IRE each month. NAEFS ensemble means were used rather than the ensemble members for this research. The formula used in this study follows as:

$$\text{IRE Spread} = |Obs - Day_n| \quad (4)$$

where "Obs" is the corresponding observed IRE value for the day being tested, and n represents 1, 4, 7, or 10 where Day_n represents Day 1, 4, 7, or 10 of the forecasts for "Obs." These values were used to help identify threshold values for whether the projected IRE values represented a "HIT" or a "MISS."

Figures 1-4 shows the absolute value of the difference between the observed IRE and the NAEFS ensemble mean by month from August 2018 to February 2019 for the forecast days of 1, 4, 7, and 10:

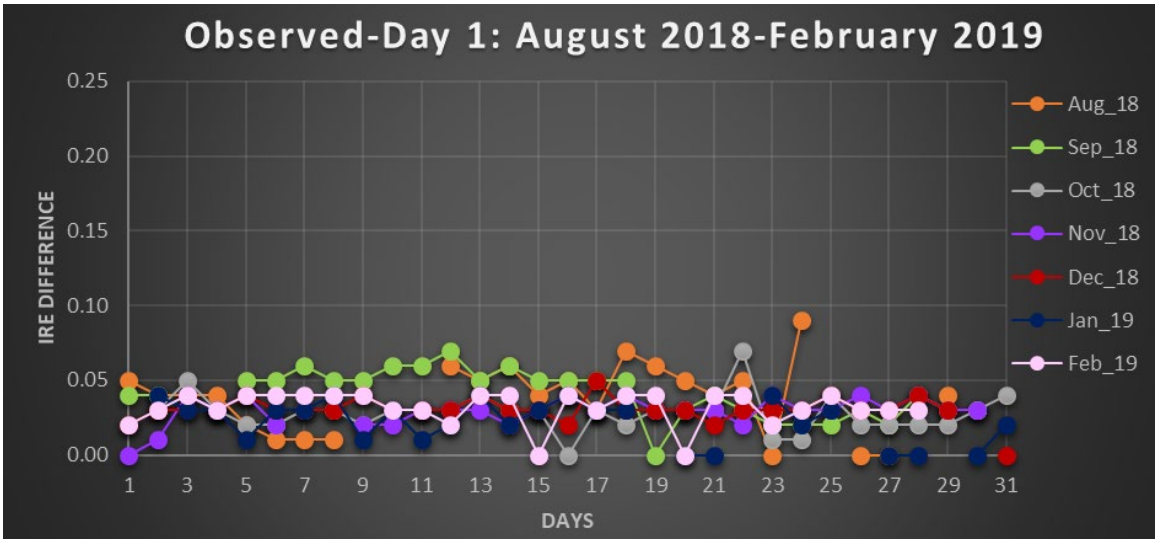

Figure 1: Absolute value of the difference between the observed IRE and Day 1 forecast NAEFS ensemble mean IRE for each month from August 2018 to February 2019.

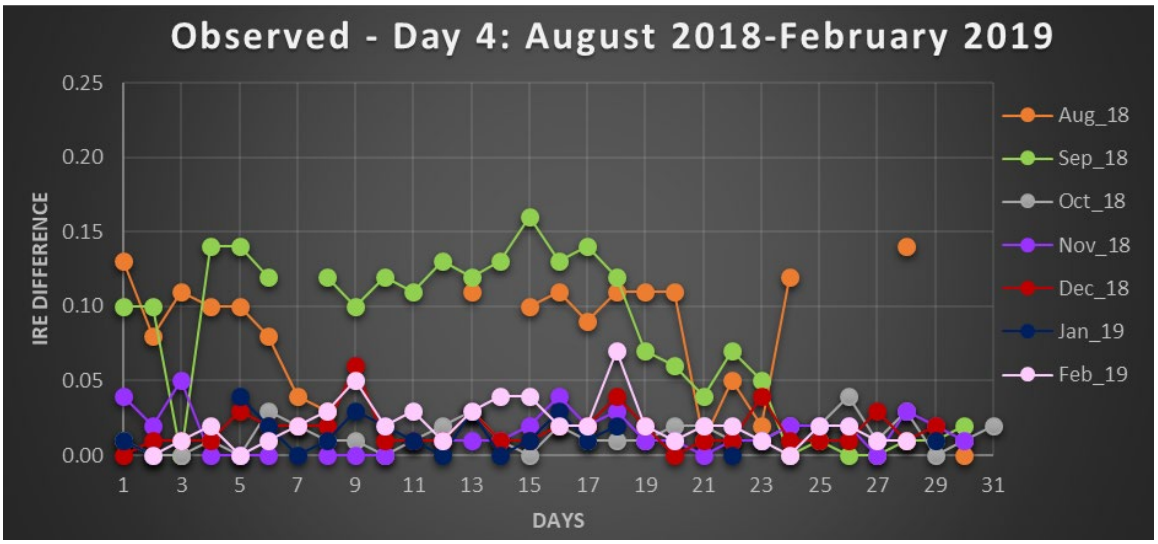

Figure 2: As in Figure 1, except for the Day 4 forecast NAEFS ensemble mean.

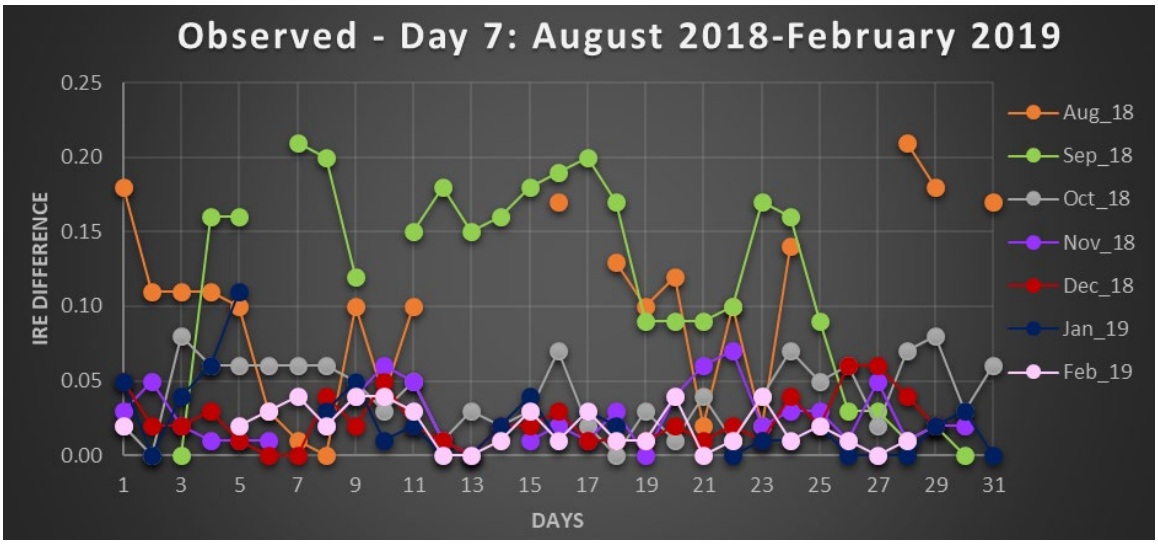

Figure 3: As in Figure 1, except for the Day 7 forecast NAEFS ensemble mean.

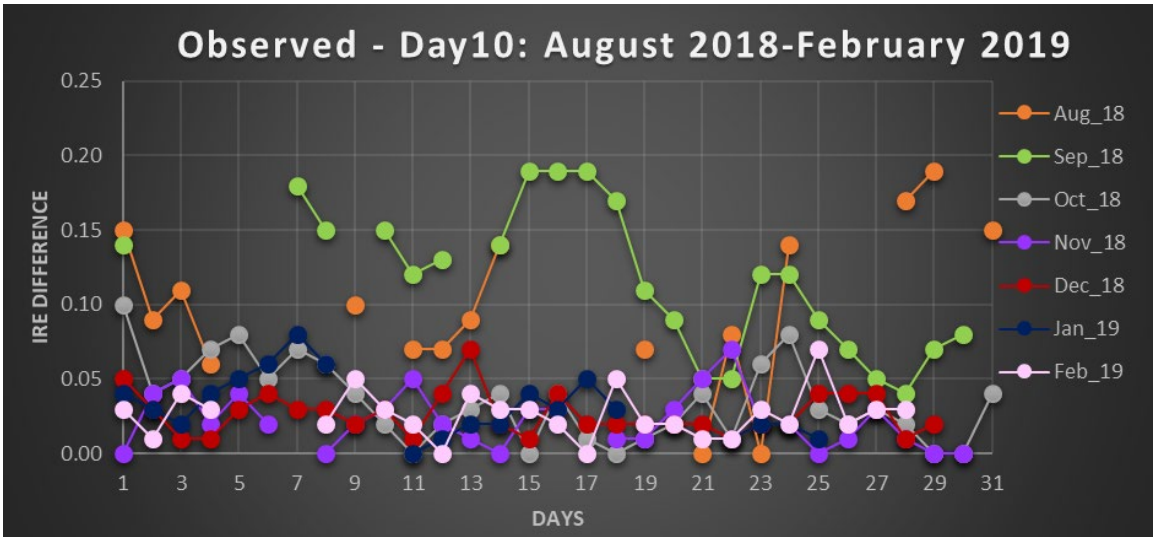

Figure 4: As in Figure 1, except for the Day 10 forecast NAEFS ensemble mean.

To attain the threshold values, Day 1, 4, 7, and 10, for each month was averaged together in their respective groups (i.e., Obs - Day 1, Obs – Day 4, etc). The threshold values are attained from means for each month for each group, as listed above. Figures 5-11 are the box and whisker plots used to determine the IRE threshold values to determine forecast skill:

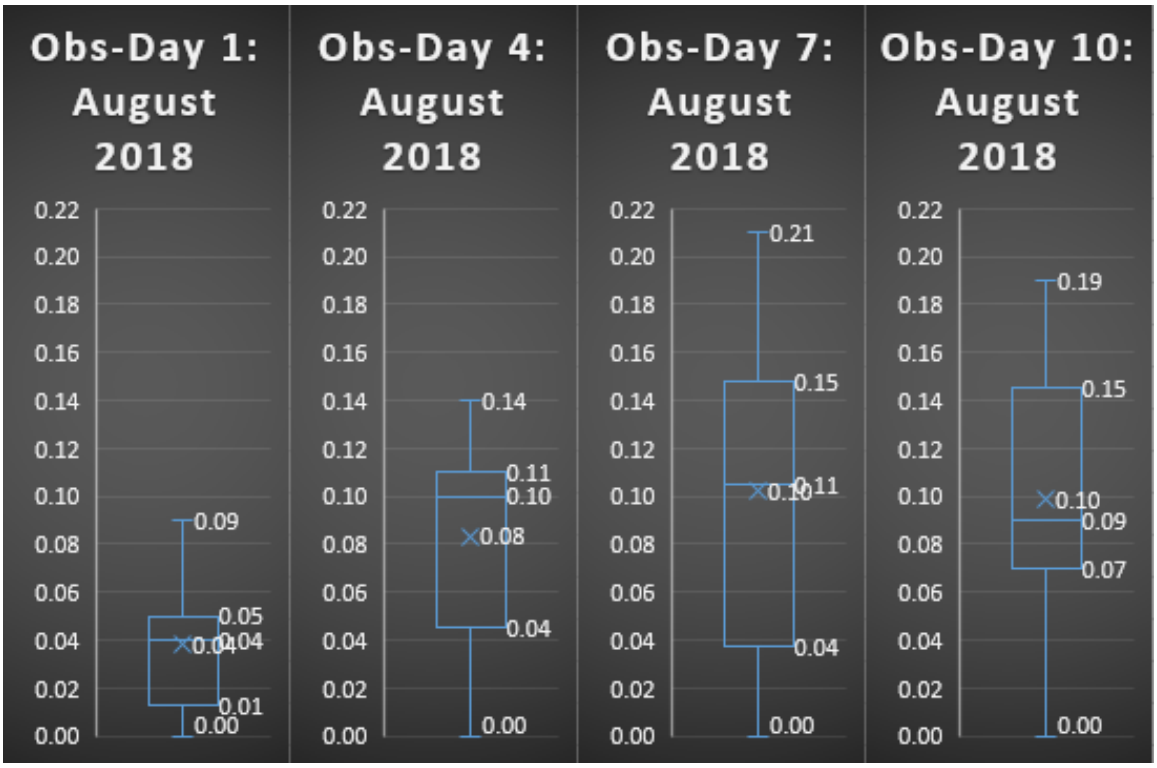

Figure 5: Tukey box and whisker plot [43] for August 2018 IRE spread calculations.

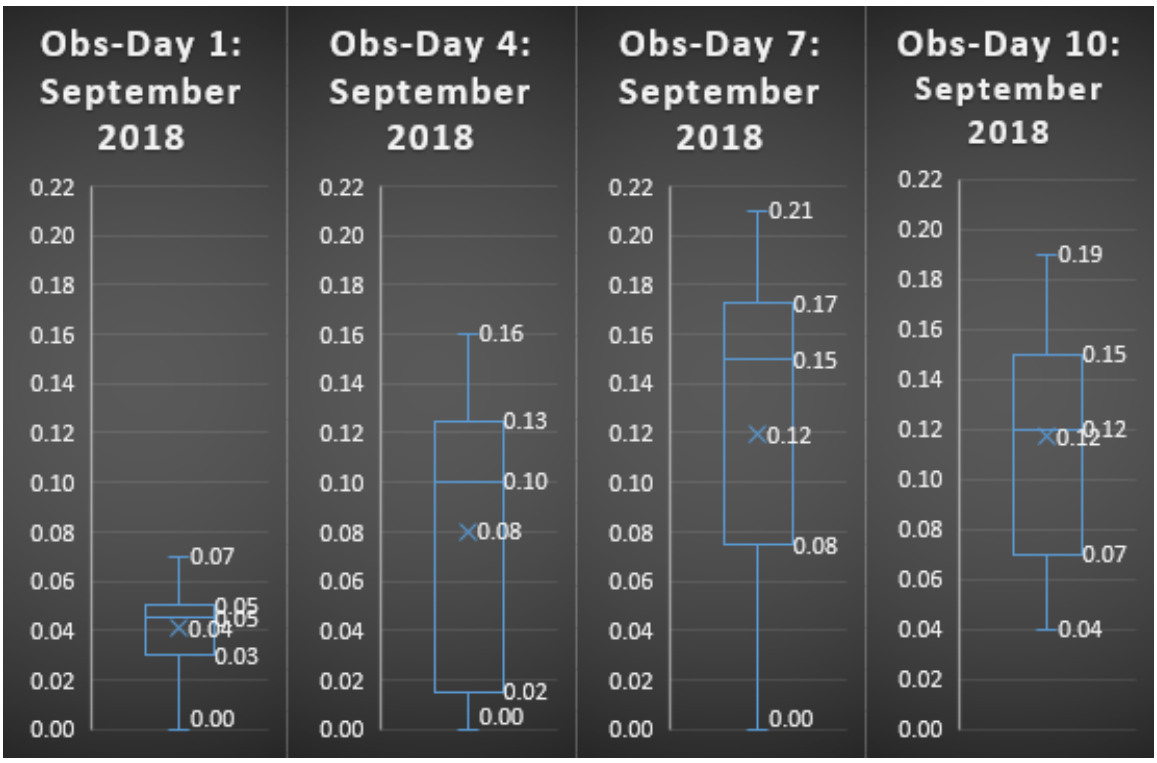

Figure 6: As in Figure 5, except for September 2018.

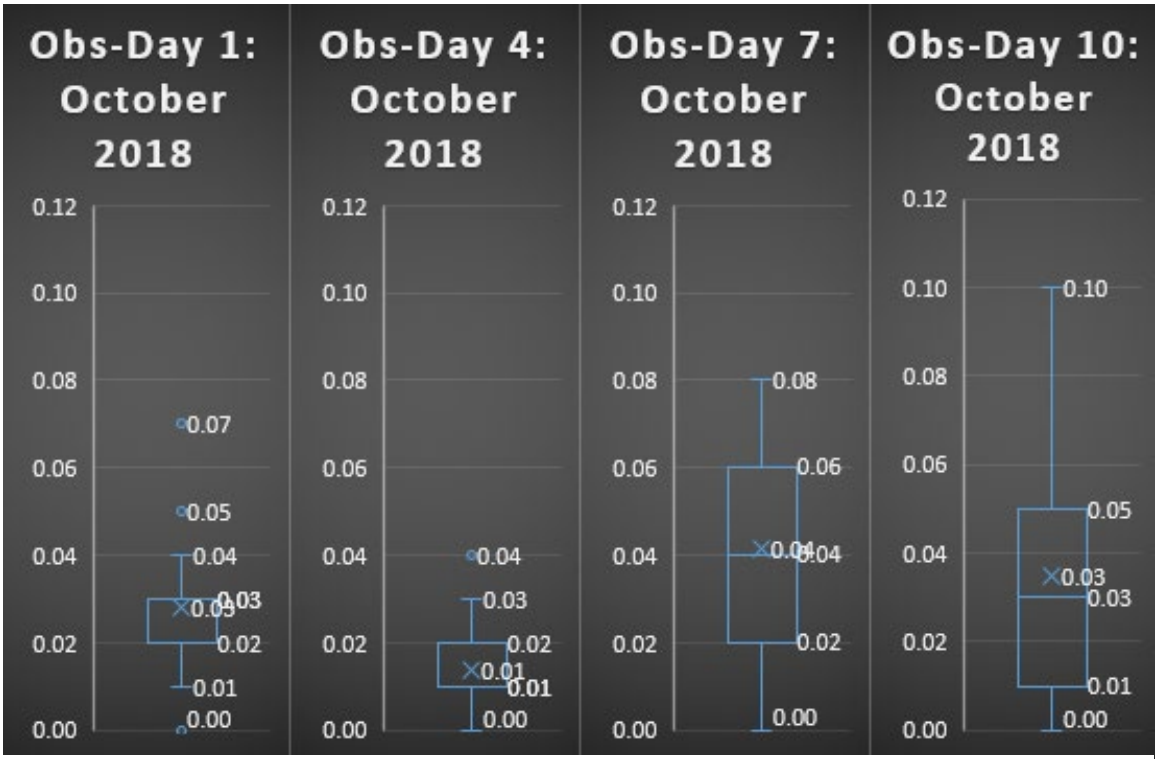

Figure 7: As in Figure 5, except for October 2018.

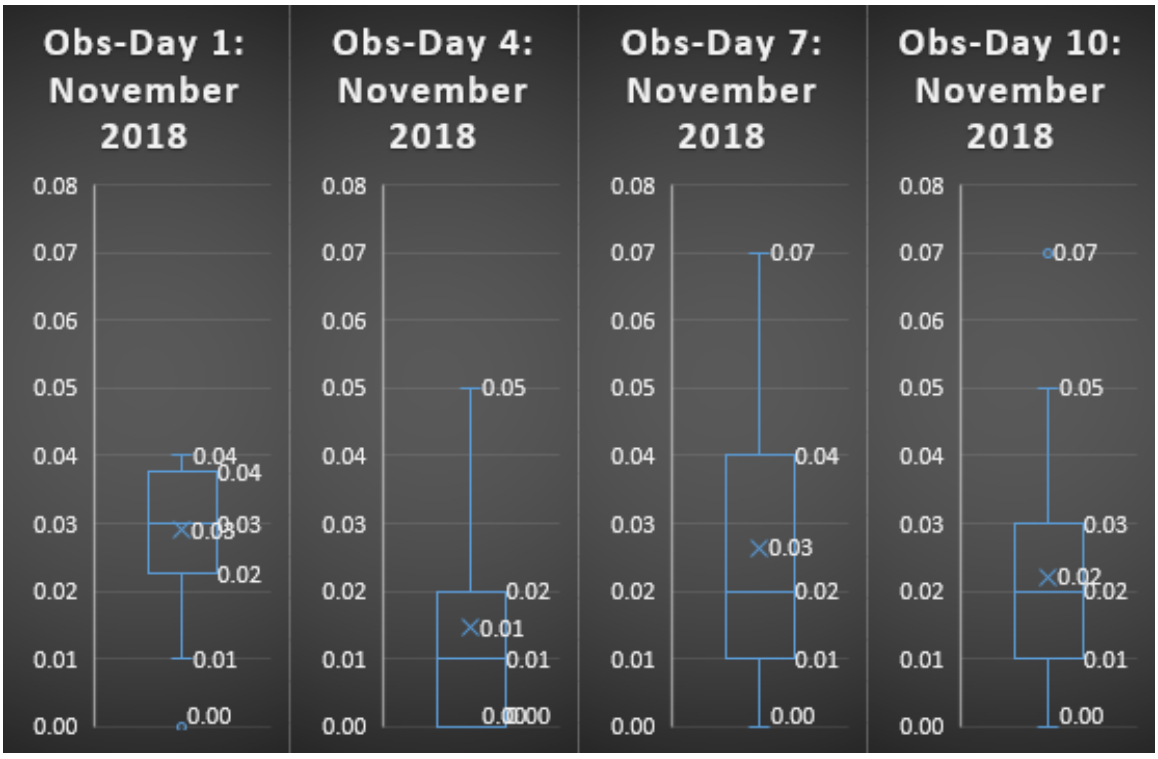

Figure 8: As in Figure 5, except for November 2018.

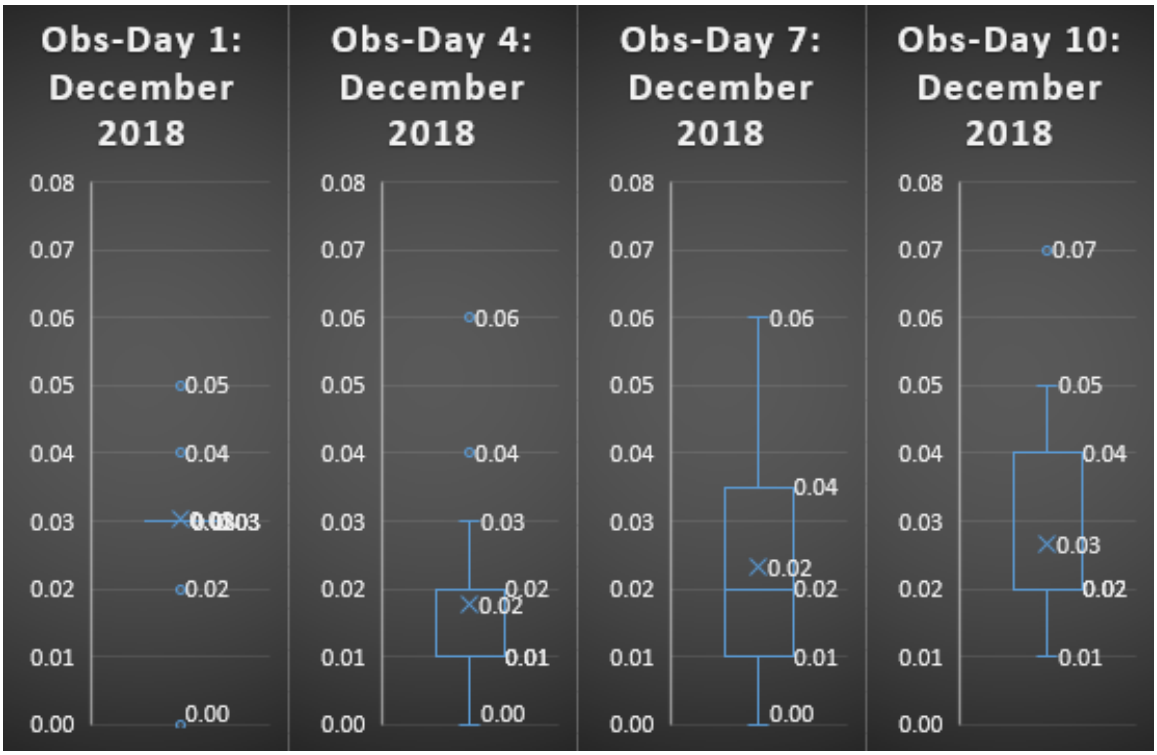

Figure 9: As in Figure 5, except for December 2018.

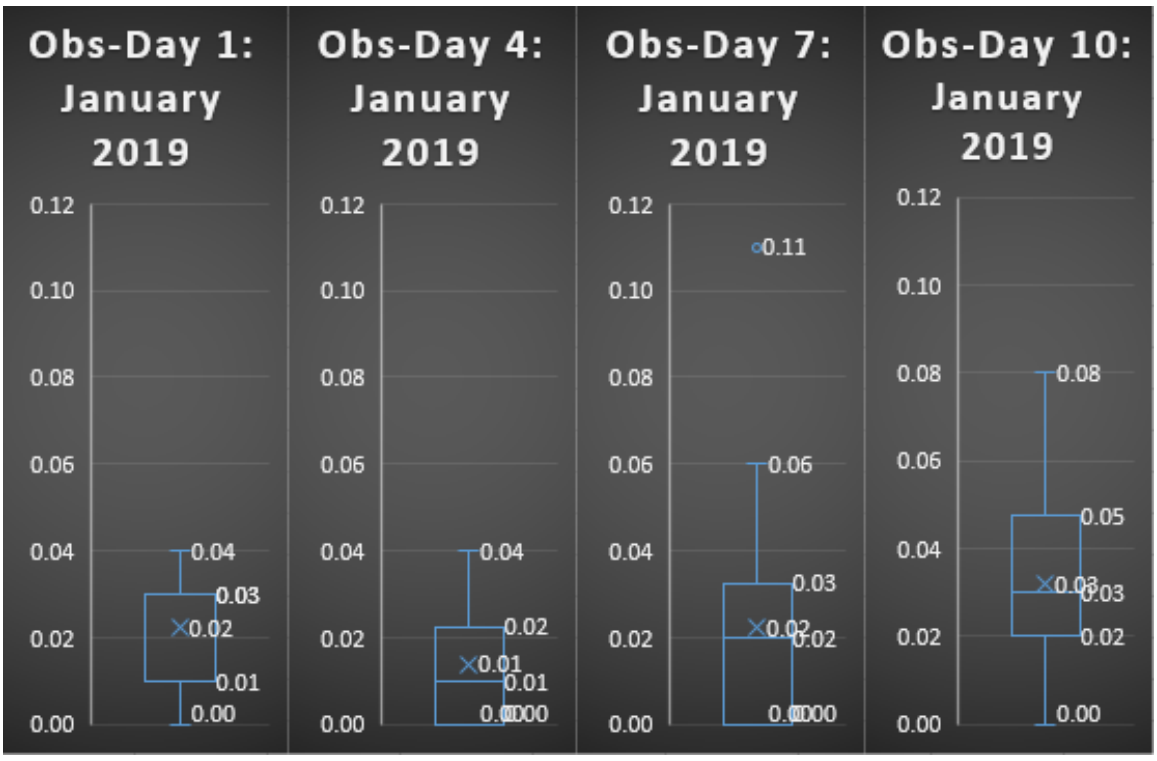

Figure 10: As in Figure 5, except for January 2019.

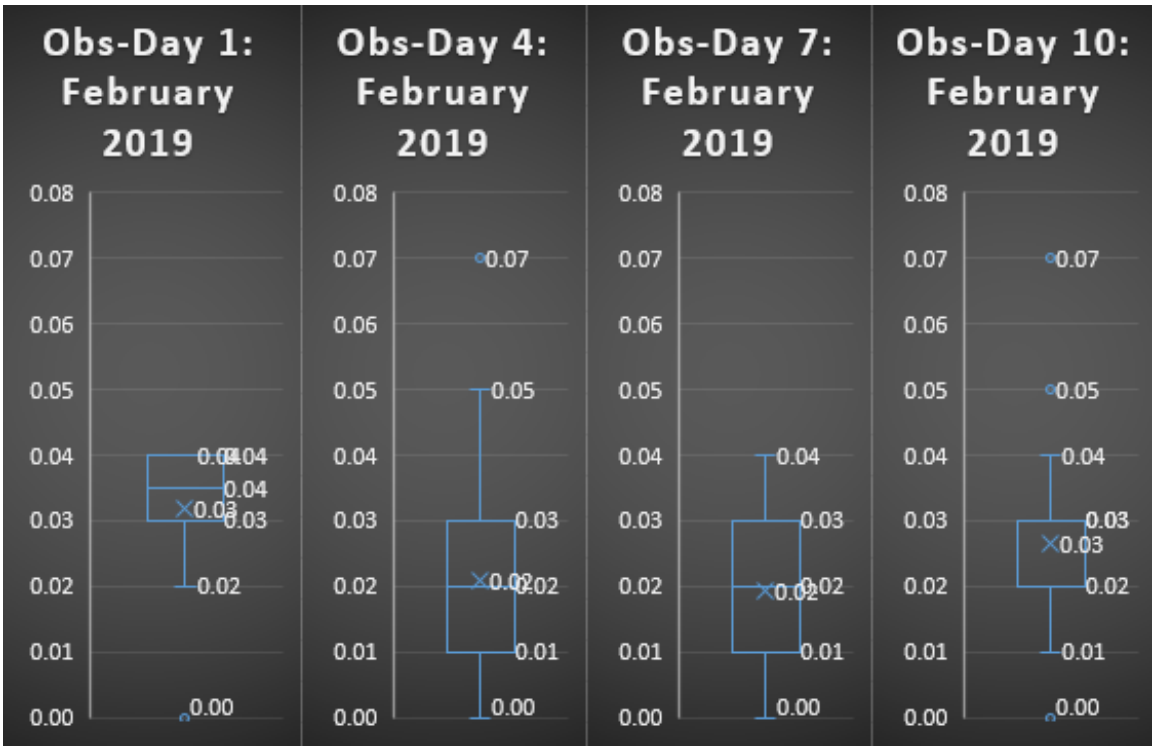

Figure 11: As in Figure 5, except for January 2019.

If the absolute value of the difference of the observed IRE minus the respective forecast day fell beneath or was equal to the determined threshold value for the event being tested, or:

$$\text{IRE Spread} \leq Day_n \text{ Threshold} \quad (5)$$

where n represents 1,4,7, or 10, then the forecast was deemed a HIT. If the value was above the threshold, or:

$$\text{IRE Spread} > Day_n \text{ Threshold} \quad (6)$$

the forecast was deemed a MISS. If the event fell under the HIT criteria, but there were no blocking onset/decay, any blocking in general, or any other regime transition anomalies (such as significant high and low pressure anomalies onsetting or decaying in the Northern Hemisphere), then the event was considered a FALSE ALARM.

Table 2 lists each months' threshold criteria for determining whether day 1, 4, 7 or 10 was a HIT or MISS:

IRE Threshold Values for Testing Skill							
August 2018		**September 2018**		**October 2018**		**November 2018**	
Obs-Day 1:	0.04	**Obs-Day 1:**	0.05	**Obs-Day 1:**	0.03	**Obs-Day 1:**	0.03
Obs-Day 4:	0.10	**Obs-Day 4:**	0.10	**Obs-Day 4:**	0.01	**Obs-Day 4:**	0.01
Obs-Day 7:	0.11	**Obs-Day 7:**	0.15	**Obs-Day 7:**	0.04	**Obs-Day 7:**	0.02
Obs-Day 10:	0.09	**Obs-Day 10:**	0.12	**Obs-Day 10:**	0.03	**Obs-Day 10:**	0.02
December 2018		**January 2019**		**February 2019**			
Obs-Day 1:	0.03	**Obs-Day 1:**	0.02	**Obs-Day 1:**	0.04		
Obs-Day 4:	0.02	**Obs-Day 4:**	0.01	**Obs-Day 4:**	0.02		
Obs-Day 7:	0.02	**Obs-Day 7:**	0.02	**Obs-Day 7:**	0.02		
Obs-Day 10:	0.03	**Obs-Day 10:**	0.03	**Obs-Day 10:**	0.03		

Table 2: IRE thresholds values for each month from August 2018 to February used to test IRE skill according to each month.

In order to determine which events to test IRE skill, each observed IRE value was subtracted from the previous day's observed IRE value to identify 24-hour spikes or drops in IRE. Figures 12-18 shows our findings:

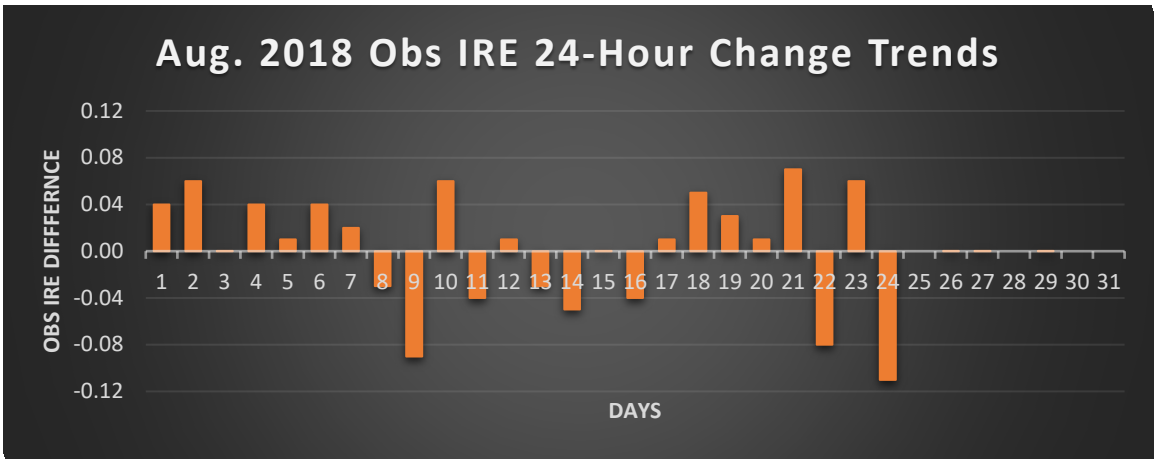

Figure 12: The 24-hour difference for the observed IRE minus the previous day observed IRE for August 2018.

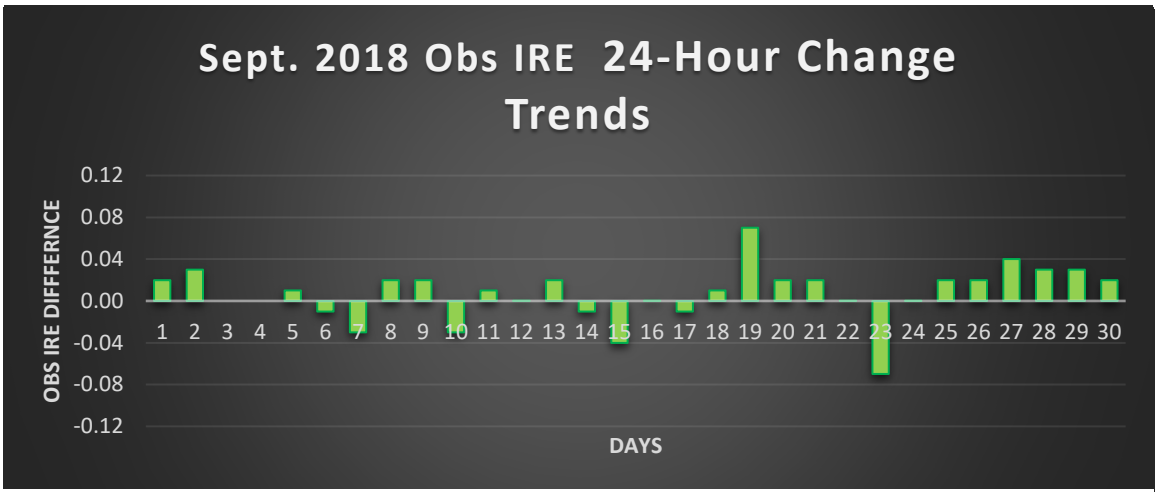

Figure 13: As in Figure 12, except for September 2018.

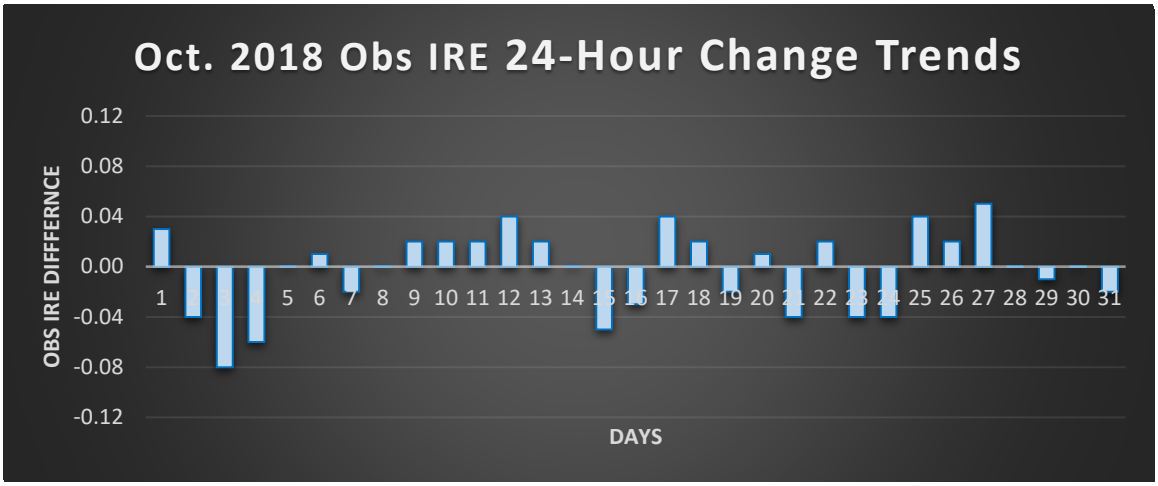

Figure 14: As in Figure 12, except for October 2018.

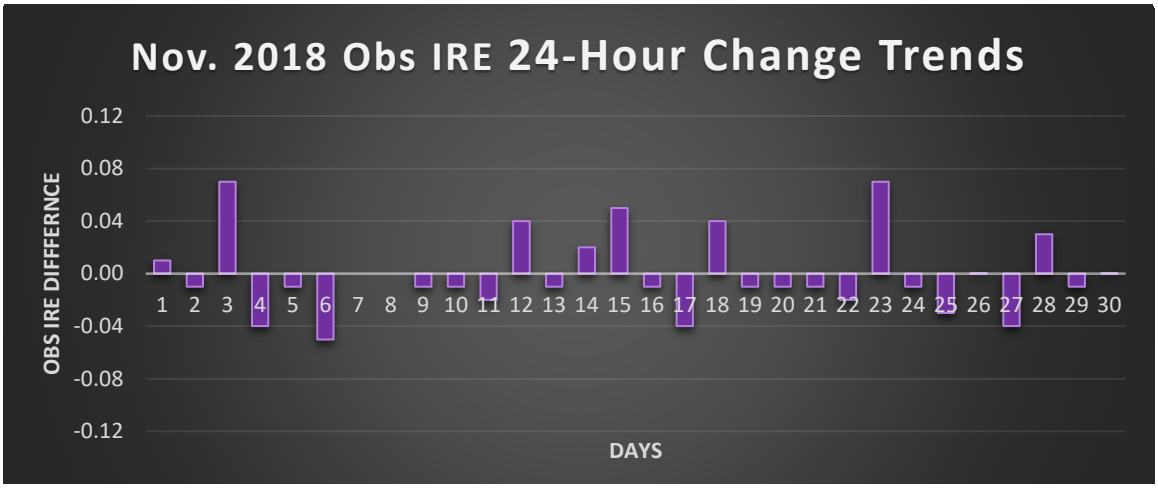

Figure 15: As in Figure 12, except for November 2018.

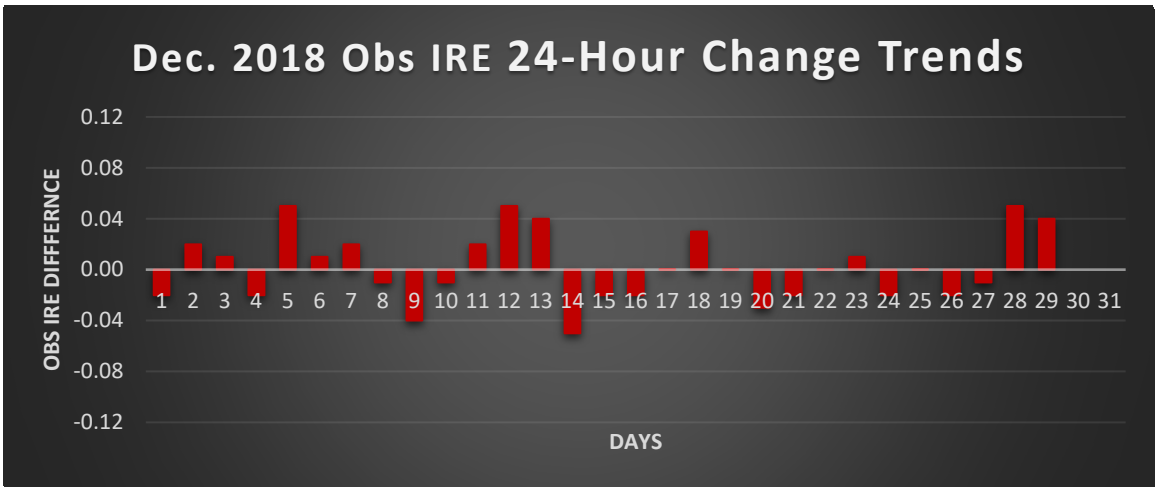

Figure 16: As in Figure 12, except for December 2018.

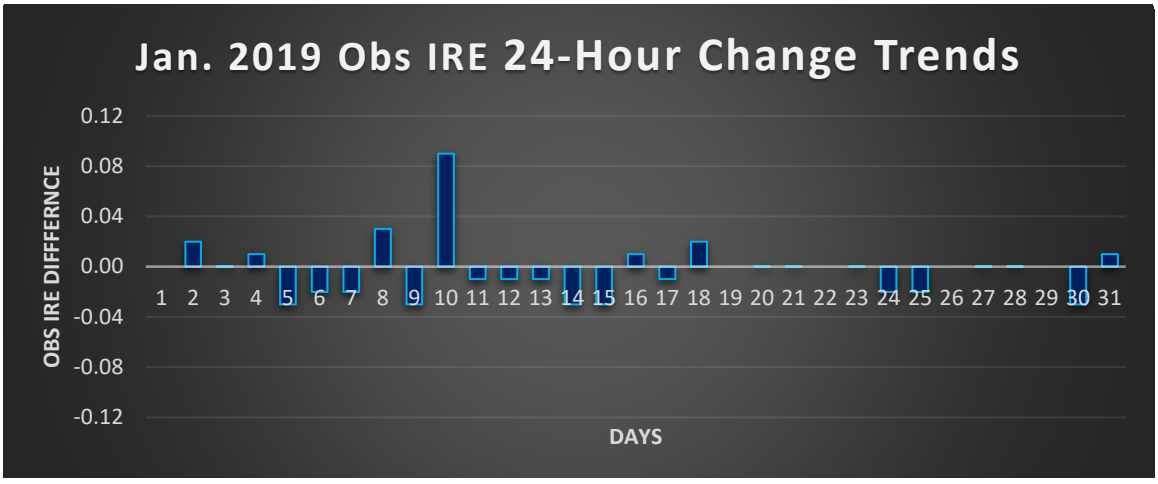

Figure 17: As in Figure 12, except for January 2019.

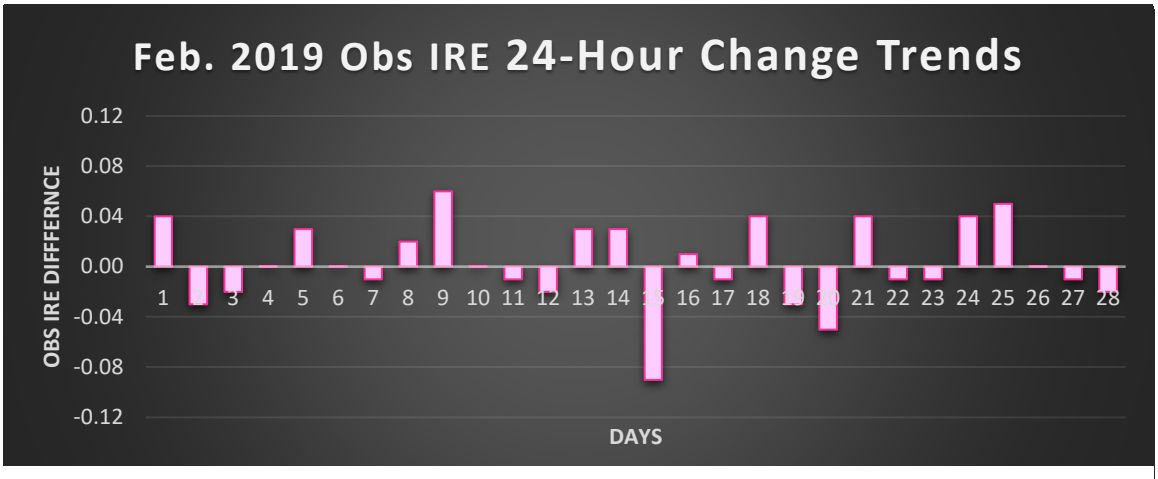

Figure 18: As in Figure 12, except for February 2019.

This method was used on the observed IRE values from the months of August 2018 through February 2019. Previous months were not used since there was either little to no observed IRE data in each month up until August 2018. This method suggested that a 0.07 increase or decrease in IRE over 24-hours was a significant spike or drop in IRE, suggesting potential regime transition. The following are all of the events from August 2018 through February 2019 that had a 0.07 increase or decrease in observed IRE over 24-hours:

- 9 August 2018 with a 0.09 decrease
- 21 August 2018 with a 0.07 decrease
- 22 August 2018 with a 0.08 decrease
- 24 August 2018 with a 0.11 decrease
- 22 September 2018 with a 0.07 increase
- 23 September 2018 with a 0.07 decrease
- 3 October 2018 with a 0.08 decrease
- 3 November 2018 with a 0.07 increase
- 23 November 2018 with a 0.07 IRE increase

Another method to find events that could indicate potential regime transition to testing IRE forecasting skill was if the observed IRE value was abnormally high (i.e., in the top 3 observed IRE values). There were 3 significant events with unusually high IRE values in our dataset, which included:

- 1 October 2018 with the second highest observed IRE of 0.84 $km^2 \cdot s^{-2}$
- 14 February 2019 with the highest observed IRE value of 0.85 $km^2 \cdot s^{-2}$ and a 0.09 increase in observed IRE over a 24-hour period
- 25 February 2019 with the 3rd highest observed IRE of 0.83 $km^2 \cdot s^{-2}$.

Other events are also considered in this study, including 10 January 2019 and 22 January 2019. January 10th involved a large snowstorm in the Midwest and a 0.09 increase in observed IRE over a 24-hour period, and January 22nd involved a drastic drop in temperatures across most of the United States, resulting in unseasonably cold conditions for a few days.

After applying the threshold values according to Table 2 to the observed IRE for each of the above events, we chose six out of the list to demonstrate IRE skill. The following events are:

- 21 August 2018 (FALSE ALARM)
- 24 August 2018 (MISS)
- 19 September 2018 (FALSE ALARM)
- 23 September 2018 (HIT)
- 14 February 2019 (MISS)
- 25 February 2019 (HIT)

In each case, blocking onset, decay, and maintenance was analyzed, along with the increase/decrease in 24-hour IRE change, the observed IRE, and any other significant weather events (e.g. onset of a major hurricane).

Chapter 3: Results and Discussion

3.1 FALSE ALARM Case: 21 August 2018

This event was analyzed due to a 0.07 drop in observed IRE over 24 hours. Due to this shift, we analyzed the potential for regime transition and blocking onset/decay. Our 500-hPa heights map for this date, shown in Figure 19, shows a subjective wave pattern of five, with low pressure centers over west-central Russia, eastern Russia, and right off the coast of eastern Russia. High pressure sits over the Mediterranean Sea near Italy, while high pressure sits over the CONUS. The maximum 500-hPa height was observed at 5975-m while the minimum was observed at 5278-m.

21 August 2018 - FALSE ALARM	
Reason for significance:	0.07 IRE drop
Observed IRE:	0.74 $km^2 \cdot s^{-2}$
Blocking:	No blocking
Day 1	FALSE ALARM
Day 4	FALSE ALARM
Day 7	FALSE ALARM
Day 10	FALSE ALARM

Table 3: Information for 21 August 2018 False Alarm case.

The observed IRE for this day was 0.74 $km^2 \cdot s^{-2}$, with Day 1, 4, 7, and 10 qualifying as HITs for regime transition in the Northern Hemisphere, as shown in Table 3. Day 1's projection of the observed IRE was 0.04 units away at 0.70, qualifying as a HIT (see table 2 for the threshold values). Day 4's projection of the observed IRE was 0.01 units away at 0.75, also qualifying as a HIT. Day 7's projection of the observed IRE was 0.02 units away at 0.76, also qualifying as a HIT. Day 10's projection of the observed IRE accurately predicted the value at 0.74, also qualifying as a HIT. In spite of observing a HIT for regime transitions, no blocking onset or decay was observed in the Northern Hemisphere for this event, nor was there any blocking already occurring. There were also no significant

geopotential height anomalies ending or beginning during this date as well, which would signify a potential large-scale regime transition. A significant geopotential height anomaly for this research is defined by a height anomaly of 180-m greater than or less than the 1981-2010 base period daily means for geopotential heights for 40° N latitude. Therefore, this event was classified as a FALSE ALARM event.

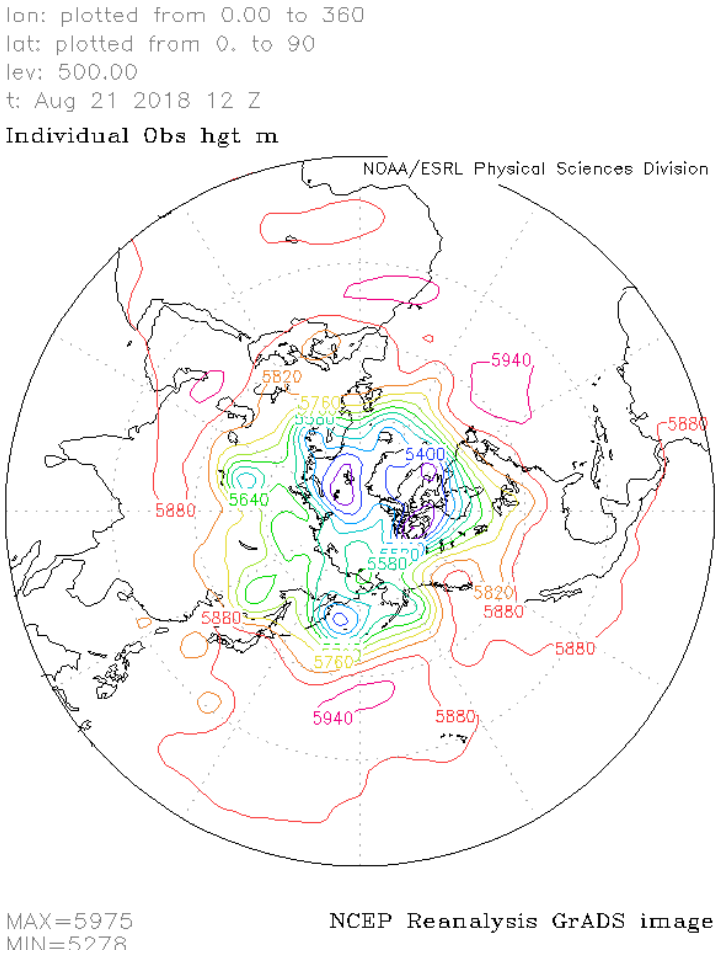

Figure 19: 500-hPA height map for 21 August 2018 at 1200 UTC.

3.2 MISS Case: 24 August 2018

Not too far from the last observed event, this date was analyzed due to a 0.11 drop in observed IRE over 24-hours. Our 500-hPa heights map of this date, shown in Figure 20, shows more active weather patterns across the Northern Hemisphere, with a wave

pattern four, arguably five. Troughs were located across western Russia, off the eastern coast of Russia over the northern Pacific, over the Norwegian Sea, and a strong low-pressure center over the Northwest Passage. The maximum 500-hPa height was observed at 5980-m while the minimum was observed at 5182-m. On top of those observations, blocking was observed on this date. On 25 August 2018 at 0000 UTC, blocking onset was observed over the Atlantic with a blocking index of 2.49. There was another blocking onset observed on 23 August 2018 at 0000 UTC over the Atlantic as well with a blocking index of 2.37.

24 August 2018 - MISS	
Reason for significance:	0.11 IRE drop
Observed IRE:	0.61 $km^2 \cdot s^{-2}$
Blocking:	Blocking starts 00UTC on 25th ends on 1st at 12UTC
Region & Blocking Index	Atlantic - BI=2.49
Region & Blocking Index	23 Aug 00UTC - 30 Aug 00UTC Atlantic - BI=2.37
Day 1	MISS
Day 4	MISS
Day 7	MISS
Day 10	MISS

Table 4: Information for 24 August 2018 False Alarm case.

The observed IRE for this day was low at 0.61 $km^2 \cdot s^{-2}$, with Day 1, 4, 7, and 10 all qualifying as a MISS for regime transition, as shown in Table 4. Day 1's projection of the observed IRE was 0.09 units away at 0.70, qualifying as a MISS. Day 4's projection of the observed IRE was 0.12 units away at 0.73, also qualifying as a MISS. Day 7's projection of the observed IRE was 0.14 units away at 0.75, also qualifying as a MISS. Day 10's projection of the observed IRE was 0.14 units away at 0.75, also qualifying as a MISS. Despite the observed blocking onset observed for this day, there were no significant geopotential height anomalies observed. This event is a good example of how dips in IRE could potentially indicate blocking despite the lack of regime transitions in the Northern

Hemisphere, though our Day 1, 4, 7, and 10 did not perform well according to our threshold values outlined in Table 2.

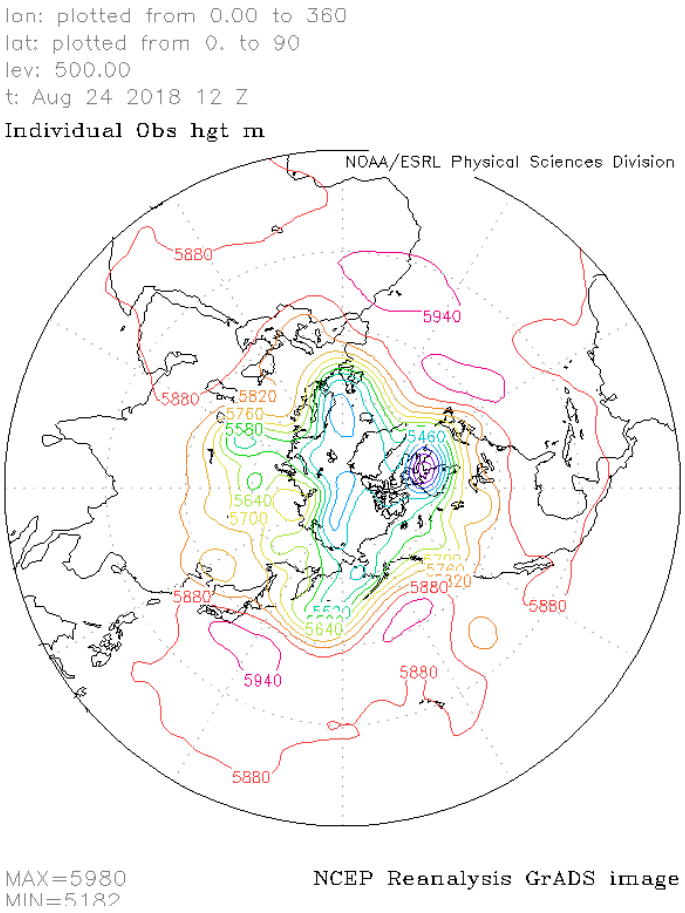

Figure 20: As in Figure 19, except for 24 August 2018.

3.3 FALSE ALARM Case: 19 September 2018

Another FALSE ALARM case was observed on this event after analyzed for a 0.07 drop in 24-hour observed IRE. Our 500-hPa heights map, shown in Figure 21, shows a subjective wave pattern five, with troughs located over western Russia, central Russia, on the eastern coast of Russia, over the northeastern Atlantic, and a strong low-pressure center

over Nunavut. The maximum 500-hPa height was observed at 5946-m while the minimum was observed at 5100-m.

19 September 2018 - FALSE ALARM	
Reason for significance:	0.07 IRE rise
Observed IRE:	0.68 $km^2 \cdot s^{-2}$
Blocking:	No blocking
Day 1	FALSE ALARM
Day 4	FALSE ALARM
Day 7	FALSE ALARM
Day 10	FALSE ALARM

Table 5: Information for 19 September 2018 False Alarm case.

The observed IRE for this day was measured at 0.68 $km^2 \cdot s^{-2}$, with Day 1, 4, 7, and 10 qualifying as HITs, as shown in Table 5. Day 1's projection of the observed IRE accurately predicted the value at 0.68, qualifying as a HIT for regime transition. Day 4's projection of the observed IRE was 0.07 units away at 0.75, also qualifying as a HIT. Day 7's projection of the observed IRE was 0.09 units away at 0.77, also qualifying as a HIT. Day 10's projection of the observed IRE was 0.11 units away at

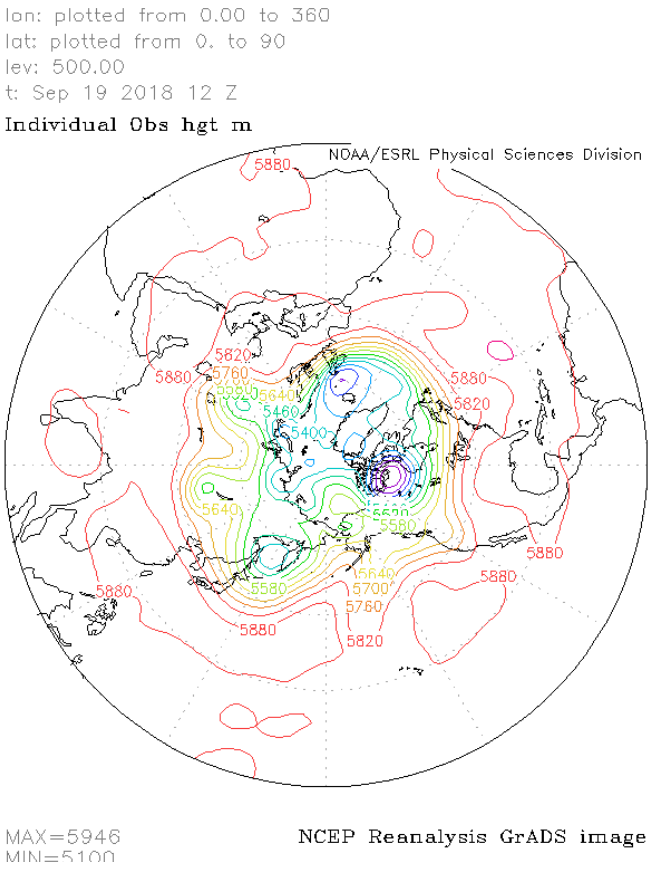

Figure 21: As in Figure 19, except for 19 September 2018.

0.79, also qualifying as a HIT. Similar to the 21 August 2018 case, there was no observed blocking onset or decay in the northern hemisphere, nor were there any significant geopotential height anomalies ending or beginning in the Northern Hemisphere. There was also no already occurring blocking events occurring at this time, either. Therefore, the event was classified as a false alarm.

3.4 HIT Case: 23 September 2018

This event was analyzed due to a 0.07 observed IRE drop within 24-hours. Our 500-hPa heights map, shown in Figure 22, shows a subjective wave pattern of six, with troughs existing over west-central Russia, eastern Russia over the north-central Pacific, over the southwest corner of Canada and northwest CONUS, over Baffin Bay into the Labrador Sea, and over Western Europe. The maximum 500-hPa height was observed at 5959-m while the minimum was observed at 5105-m. Blocking onset was also observed on 23 September 2018 at 0000-UTC over the Pacific Ocean with a blocking index of 3.82. Another special note about this event was that Hurricane Leslie also begin on 23 September 2018. This tropical storm eventually grew to a category 1 hurricane.

23 September 2018 - HIT	
Reason for significance:	0.07 IRE drop
Observed IRE:	0.65 $km^2 \cdot s^{-2}$
Blocking: Region & Blocking Index	Blocking starts 00UTC on 23rd ends on Oct 3rd at 00UTC Pacific - BI=3.82
Day 1	HIT
Day 4	HIT
Day 7	MISS
Day 10	HIT

Table 6: Information for 23 September 2018 False Alarm case.

The observed IRE for this day was low at 0.65 $km^2 \cdot s^{-2}$, with Day 1, 4, and 10 all qualifying as a HIT and Day 7 qualifying as a MISS in regards to regime transitions, as

shown in Table 6. Day 1's projection of the observed IRE was 0.02 units away at 0.63, qualifying as a HIT. Day 4's projection of the observed IRE was 0.05 units away at 0.70, also qualifying as a HIT. Day 7's projection of the observed IRE was 0.17 units away at 0.82, qualifying as a MISS. Day 10's projection of the observed IRE was 0.12 units away at 0.77, also qualifying as a HIT. This event is considered a HIT since Days 1 and 4 qualified as HITS, and the majority of the tested days qualified as HITs as well. Considering there were no significant geopotential height anomalies observed for this day, this event is a good example of predicting regime transition not only in the form of blocking onset, but with tropical storm development.

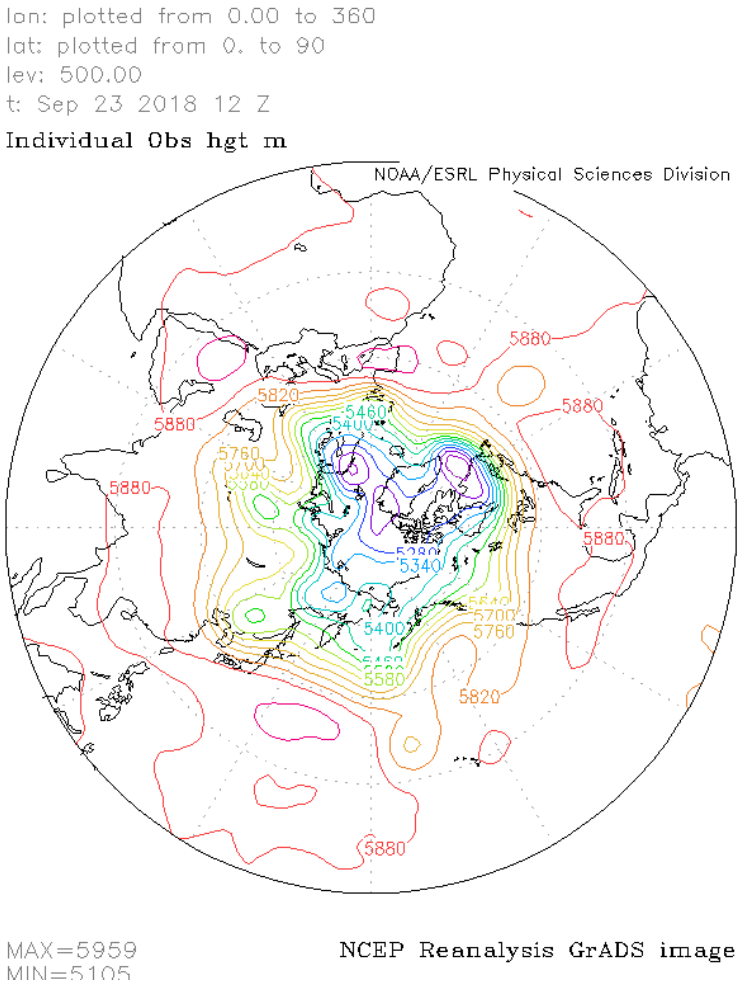

Figure 22: As in Figure 19, except for 23 September 2018.

3.5 MISS Case: 3 November 2018

Much like the event described above, this event was also observed due to a 0.07 observed IRE rise within 24-hours. Our 500-hPa heights map, as shown in Figure 23, shows a subjective wave pattern of five, with troughs located over the north-central Pacific, over central Russia, over the northeastern portion of the North Atlantic, and over the CONUS. The maximum 500-hPa height was the highest observed among our cases at 5986-m while the minimum was observed at 4956-m. Blocking was also observed on 2 November 2018 over the Atlantic with a blocking index of 3.42.

3 November 2018 - MISS	
Reason for significance:	0.07 IRE rise
Observed IRE:	0.79 $km^2 \cdot s^{-2}$
Blocking:	Blocking starts 00UTC on 2nd ends on Nov 15th at 00UTC Atlantic - BI=3.42
Day 1	MISS
Day 4	MISS
Day 7	HIT
Day 10	MISS

Table 7: Information for 3 November 2018 False Alarm case.

The observed IRE for this day was low at 0.79 $km^2 \cdot s^{-2}$, with Day 1, 4, and 10 all qualifying as a MISS and Day 7 qualifying as a HIT in regards to regime transition, as shown in Table 7. Day 1's projection of the observed IRE was 0.04 units away at 0.75, qualifying as a MISS. Day 4's projection of the observed IRE was 0.05 units away at 0.74, also qualifying as a MISS. Day 7's projection of the observed IRE was 0.02 units away at 0.77, qualifying as a HIT. Day 10's projection of the observed IRE was 0.05 units away at 0.74, also qualifying as a MISS. This event is considered a MISS since the majority of the day projections qualified as a MISS, but most importantly that Day 1 and 4 were a MISS as well. Blocking onset was observed for this day, though our IRE projections did not fall within the thresholds in Table 2. Despite there not being any significant

geopotential height anomalies for this day, this event is still classified as a MISS for missing the blocking onset.

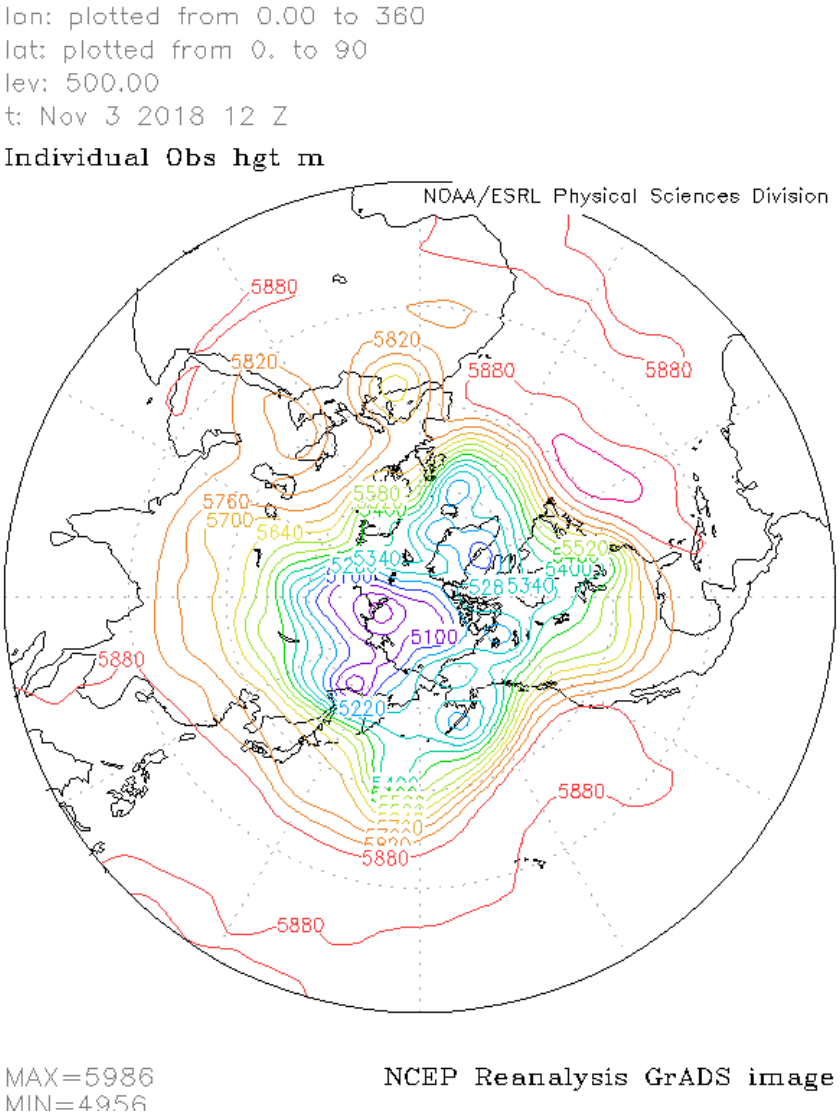

Figure 23: As in Figure 19, except for 3 November 2018.

3.6 HIT Case: 14 February 2019

Not only did this event demonstrate a 0.09 rise in observed IRE in 24-hours, but this event measured the highest observed IRE in our dataset. Our 500-hPa heights maps, shown in Figure 24, shows a wave pattern of six in the Northern Hemisphere with comparatively larger troughs over the western Pacific Ocean, over eastern Canada, over the eastern

portion of the North Atlantic Ocean, over the Middle East, and over eastern Russia and the northwest Pacific Ocean. The maximum 500-hPa height was observed at 5920-m while the minimum was our lowest observed in our cases at 4767-m. Blocking onset was also observed on 14 February 2019 at 0000-UTC over the Atlantic with a blocking index of 2.09. Another block was also occurring at this time between the dates of 11 February 2019 through 17 February 2019 over the Pacific with a blocking index of 3.8.

14 February 2019 - HIT	
Reason for significance:	Highest IRE in dataset
Observed IRE:	0.85 $km^2 \cdot s^{-2}$
Blocking:	Blocking starts 00UTC on 14th ends on Feb 20th at 00UTC
Region & Blocking Index	Atlantic - BI=3.09
Region & Blocking Index	Feb 11 00UTC - 17 00UTC Pacific - BI=3.8
Day 1	HIT
Day 4	HIT
Day 7	HIT
Day 10	HIT

Table 8: Information for 14 February 2019 False Alarm case.

The observed IRE for this day was high at 0.85 $km^2 \cdot s^{-2}$, with Day 1, 4, 7, and 10 all qualifying as a HIT in regards to regime transition, as shown in Table 8. Day 1's projection of the observed IRE was 0.04 units away at 0.81, qualifying as a HIT. Day 4's projection of the observed IRE was 0.04 units away at 0.81, also qualifying as a HIT. Day 7's projection of the observed IRE was 0.01 units away at 0.84, also qualifying as a HIT. Day 10's projection of the observed IRE was 0.03 units away at 0.82, also qualifying as a HIT. Not only was blocking onset and maintenance observed for this day, but we also observed a significant positive geopotential height anomaly of 300-m above 1981-2010 base period daily mean for geopotential heights ending between February 14-15 in the central Pacific, and a negative geopotential height anomaly of 180-m beginning on 14 February 2019 off the west coast of North America. These two events qualify as large-scale regime

transitions, and with these two regime transitions along with the blocking onset and maintenance shows this specific event's competency in forecasting for regime transition and blocking onset.

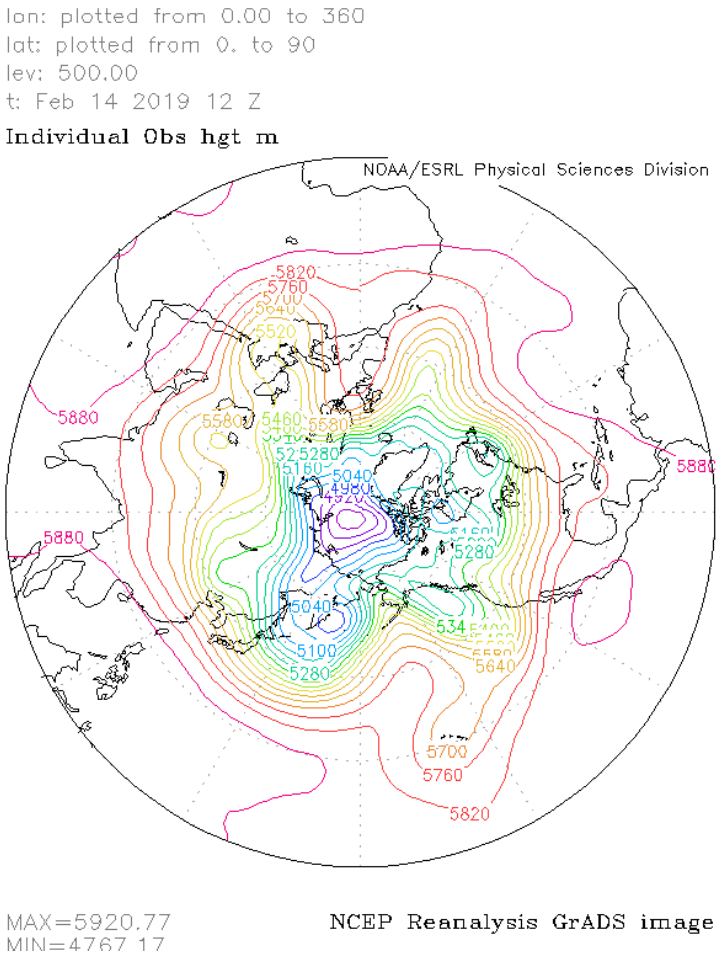

Figure 24: As in Figure 19, except for 14 February 2019.

3.7 Discussion

The most noticeable trend with testing IRE skill was the large spread of results between observed IRE and its projected forecast days throughout the seasons. The months of August 2018 and September 2018 had the largest thresholds out of our August 2018 through February 2019 dataset (see Table 2). For both August and September, we see Day

1's spread ranging from 0.00 to above 0.05 while all October through February's Day 1 spread sat between 0.00 or 0.01 and 0.04, as seen in Figures 5-11. And as expected, Day 4, 7, and 10's spreads grew larger as the forecast projected farther into time, shown in Figures 5-11.

For Day 4 projections, August 2018's spread was between 0.00 and 0.14, September 2018's spread was between 0.00 and 0.16, October 2018's spread was between 0.00 and 0.03 with one outlier of 0.04, November 2018's spread was between 0.00 and 0.05, December 2018 spread was between 0.00 and 0.03 with two outliers of 0.04 and 0.06, January 2019's spread was between 0.00 and 0.04, and February's spread was between 0.00 and 0.05 with one outlier of 0.07. For Day 7 projections, August 2018's spread was between 0.00 and 0.21, September 2018's spread was between 0.00 and 0.21, October 2018's spread was between 0.00 and 0.08, November 2018's spread was between 0.00 and 0.07, December 2018 spread was between 0.00 and 0.06, January 2019's spread was between 0.00 and 0.06 with one outlier of 0.11, and February's spread was between 0.00 and 0.04. For Day 10 projections, August 2018's spread was between 0.00 and 0.19, September 2018's spread was between 0.04 and 0.19, October 2018's spread was between 0.00 and 0.10, November 2018's spread was between 0.00 and 0.05 with one outlier of 0.07, December 2018 spread was between 0.01 and 0.05 with one outlier of 0.07, January 2019's spread was between 0.00 and 0.08, and February's spread was between 0.01 and 0.04 with three outlier of 0.00, 0.05, and 0.07.

We can draw a couple of assumptions from these results. The first being that between the months of October 2018 and February 2019, overall GEFS's NAEFS projected values closer to the observed IRE than compared to the warmer months of August 2018 and

September 2018. The second assumption we can draw from this is that Day 1 projections of the observed IRE performed overall better than Day 4, 7, and 10, and Day 4 projections performed better overall than Day 7 and 10.

Sixteen total events were tested for IRE skill, which were where our six discussed cases were selected from. Cases to be discussed in this paper were selected if all of the skill classifications (HITs, MISS's, or FALSE ALARMs) were the same between Day 1, 4, 7, and 10, or if three out of the four were the same. Table 9 shows the HITs, MISS's, and FALSE ALARMs for each month for each forecast day:

Number of HITs, MISS's, and FALSE ALARMs for Each Event Each Month							
August 2018		**September 2018**		**October 2018**		**November 2018**	
HIT	4	**HIT**	4	**HIT**	3	**HIT**	4
MISS	6	**MISS**	4	**MISS**	4	**MISS**	4
FALSE ALARM	4	**FALSE ALARM**	4	**FALSE ALARM**	0	**FALSE ALARM**	0
December 2018		**January 2019**		**February 2019**			
HIT	1	**HIT**	4	**HIT**	7		
MISS	3	**MISS**	2	**MISS**	1		
FALSE ALARM	0	**FALSE ALARM**	0	**FALSE ALARM**	0		

Table 9: Number of HITs, MISS's, and FALSE ALARMs for each forecast day according to each month from August 2018 to February 2019.

Between August 2018 and December 2018, our MISS's are either equal to or greater than our HITs. But as we move into January and February 2019, that's we noticed our HITs outnumbering our MISS's. The significance behind this trend is that with higher IRE values observed in the winter months of our dataset, we would expect less predictability. Though this trend along with smaller IRE skill threshold during the winter months suggests IRE's competency in projecting observed IRE values, therefore suggesting to be a reliable indicator of regime transitions.

Our 21 August 2018 FALSE ALARM case forecasts for Day 1, 4, 7, and 10 were all within 0.04 or lower of the observed IRE, deeming this case a HIT. Upon further

investigation, no blocking onset or decay was observed, nor was there any blocking maintenance observed. To couple these observations, 500-hPa height anomalies in the NH were significantly lacking. Therefore, we deemed this case a FALSE ALARM since we had no observations of regime transition or blocking onset/decay. Our second FALSE ALARM case (19 September 2018) had a larger threshold set in comparison to our 21 August 2018 case.

When compared to the rest of September 2018's projections of the Day 1, 4, 7, and 10 forecasts, 19 September 2018 case's forecasts were among one of the closest forecast to the observed. Similar to our first FALSE ALARM case, there was no observation of blocking onset or decay, nor was there any blocking maintenance. One thing to note was that there was small height anomaly onset on 19 August 2018 around 180° longitude, 40° latitude that deviated up to 180-m from the daily 500-hPa height mean between 1981 through 2010. Since this anomaly was comparatively not as significant as other events, this event was also deemed a FALSE ALARM. A trend that surfaced with these FALSE ALARM cases was that IRE Day 1, 4, 7, and 10 projections performed well in comparison with the rest of the events we tested.

24 August 2018 and 3 November 2018 were our two MISS cases. Our first MISS case on 24 August 2018 had a significant 0.11 observed IRE drop over 24-hours, and was among one of our lowest observed IRE of 0.61. Blocking onset was observed at 0000-UTC on 25 August 2018 over the Atlantic with a blocking index of 2.49. Our 500-hPa height anomaly map shows a minor height anomaly onsetting around 26 August 2018 at 90-100° W longitude, 40° N latitude, with heights deviating up to 180-m below the 30-year average, lasting through the end of August. This is another minor height anomaly

event compared to our winter height anomalies. Since IRE drops are usually associated with a meridional wave pattern transitioning to more of a zonal pattern, in our 500-hPa height maps we notice a weakening low pressure center over the Bering Sea along with a flattening trough over the western CONUS. Due to the combination of blocking onset and the slight transition from a meridional to zonal wave pattern in certain places in the NH, this is likely why a low IRE and 24-hour IRE drop is observed.

Our second MISS case on 3 November 2018 had a 0.07 observed IRE spike over 24 hours, where blocking maintenance was observed on 0000-UTC on 2 November 2018 until 15 November 2018. There also was a significant height anomaly observed on 3 November 2018 at 50-60° W longitude, 40° N latitude, with heights deviating up to 300-m above the 30-year average. This height anomaly is likely the reason we see this jump in IRE. Though despite this regime transition, IRE projections did not lie below the threshold amounts (see Table 2). Therefore, this case was deemed a MISS, along with our 24 August 2018 event. Both of our MISS cases' Day 1, 4, 7, and 10's projections were no more than 0.05 away from the thresholds.

23 September 2018 and 14 February 2019 were our two HIT cases. Our first HIT case on 23 September 2018 had a 0.07 observed IRE drop over 24-hours. Blocking onset began at 0000-UTC on 23 September 2018 in the Pacific with a blocking index of 3.82. Our 500-hPa height anomaly map shows a few minor height anomalies onsetting between 30° W through 10° E longitude and another 40° N latitude and 150° W, 40° N latitude. To compliment this blocking observation, our 500-hPa height maps show two cut-off lows weakening between 22 September 2018 and 24 September 2018. This is indicative

of our drop in IRE, which is why this event was deemed a HIT rather than a FALSE ALARM.

The significance behind 14 February 2019 was because it held the highest observed IRE for our dataset. Blocking onset was observed at 0000-UTC on 14 February 2019 over the Atlantic with a blocking index of 3.09. Blocking maintenance was also observed between 11 February and 17 February 2019. One notable mention about this case was the large height anomaly between 180° and 130° W longitude, 40° N latitude with a height anomaly up to 300-m above the climate average. This anomaly ended near 14 February, indicating a large regime transition for this area. 500-hPa maps also indicate two strengthening lows, one near the Okhotsk Sea off the east coast of Russia and the other off the western coast of Canada. A combination of the blocking onset, the 500-hPa anomaly map, and the 500-hPa height map showing a zonal to meridional flow pattern are why this event's high IRE is indicative of regime transitions and why this case was deemed a HIT.

Chapter 4: Conclusion

Understanding blocking, and knowing where these large flow regimes will occur and persist does aid in making forecasts for the large-scale up to ten days or more. But as we move forward, the need to improve our forecasts is imperative. Therefore, having another tool or method to forecast for regime transitions is necessary. IRE has been proven to be a reliable indicator for not only indicating blocking onset/decay, but also independently indicating regime transitions. Since IRE is a new diagnostic tool, there is still much to learn about how it forecasts for large-scale atmospheric flow. The principles behind Lyapunov exponents can be applied to the principles behind IRE as well. As IRE values grow in value, we can expect less predictability, or a more unstable atmosphere. Conversely, smaller IRE values indicate a more stable atmosphere. While there is not enough data recorded to make a climatic average or to make solid assumptions on seasonal trends with IRE, one assumption we can make from our own data is how the observed IRE behaved between August 2018 and February 2019.

As seen in Figure 25 below, we see a slow increase in observed IRE values as the months move from the warmer season into the winter. Another trend to mention are the large dips in IRE during the summer months in comparison to the winter months. The large spikes and drops in IRE are likely due to the transition seasons (autumn) since high IRE projections have been found to indicate a meridional wave pattern and low IRE projections have been found to indicate zonal wave patterns. During the midst of the

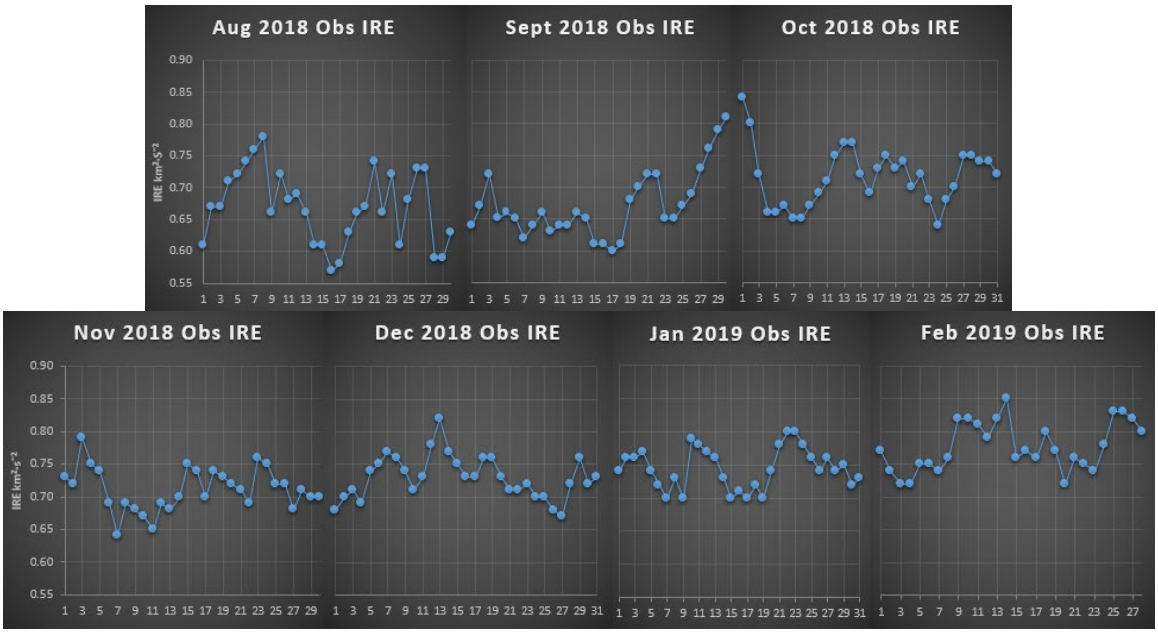

Figure 25: Observed IRE between August 2018 and February 2019.

summer and winter seasons, we see less of these spikes and high observed IRE values overall in the winter and the lower observed IRE values overall in the summer.

To better understand IRE and how it interacts with seasons and weather anomalies, further research is necessary. Connections could be found between IRE and the Madden-Julian oscillations, the Arctic Oscillation, El Nino and La Niña, seasonal patterns, and exclusively regional seasonal trends (such as severe weather season US). Upon further research, IRE could be useful for forecasting regime transitions for synoptic scale events, and potentially smaller scale events (though this is speculation and needs further research to make these assumptions). Even our FALSE ALARM events could be projecting smaller scale event that were not in the scope of this research. The MJO oscillation could potentially play a factor in in calculating IRE, as the North Atlantic Hurricane season did event a few of our event in August and September. Since our scope of research involved the entire NH, it was unfair to consider one portion of the MJO oscillation and not the rest.

Therefore as stated above, further research is necessary to find finer connections with IRE and regime transitions.

References

1. Li, Y.C. Linear hydrodynamic stability. *Notices of the American Mathematical Society.* **2018**, 65, 1255-1259.

2. Jensen, A.D.; Akperov, M.G.; Mokhov, I.I.; Lupo, A.R.; Fengpeng, S. The Dynamic Character of Northern Hemisphere Flow Regimes in a Near-Term Climate Change Projection. *Atmosphere* **2018**, 8, 12.

3. Namias, J. The great Pacific anticyclone of the winter 1948–50: A case study in the evolution of climatic anomalies. *J. Meteorol.* **1951**, 8, 251–261.

4. Lorenz, E.N. Seasonal and irregular variations of the Northern Hemisphere sea-level pressure profile. *J. Meteorol*. **1951**, 8, 52–59.

5. Wallce, J.M.; Gutzler, D.S. Teleconnections in the Geopotential Height Field during the Northern Hemisphere Winter. *Mon. Wea. Rev.*, vol 109, pp 784-812, **1981**.

6. American Meteorological Society - Weather Analysis and Forecasting. Available online: **https://www.ametsoc.org/ams/index.cfm/about-ams/ams-statements/statements-of-the-ams-in-force/weather-analysis-and-forecasting/**

7. Lupo, A.R.; Li, Y.C.; Feng, Z.C.; Fox, N.I.; Rabinowitz, J.L.; Simpson, M.L. Sensitive versus Rough Dependence under Initial Conditions in Atmospheric Flow Regimes. *Atmosphere* **2016**, 7, 11.

8. Jensen, A.D.; Lupo, A.R.; Mokhov, I.I.; Akperov, M.G.; Reynolds, D.D. Integrated Regional Enstrophy and Block Intensity as a Measure of Kolmogorov Entropy. *Atmsosphere* **2017**, 8. 10.3390/atmos8120237.

9. Dymnikov, V.P.; Kazantsev, Y.V.; Kharin, V.V. Information entropy and local Lyapunov exponents of barotropic atmospheric circulation. *Izv. Atmos. Ocean. Phys.* **1992**, 28, 425–432.

10. Lupo, A.R.; Mokhov, I.I.; Dostoglou, S.; Kunz, A.R.; Burkhardt, J.P. Assessment of the impact of the planetary scale on the decay of blocking and the use of phase diagrams and enstrophy as a diagnostic. *Izv. Atmos. Ocean. Phys.* **2007**, 43, 45–51.

11. Athar, H.; Lupo, A.R. Scale Analysis of Blocking Evens from 2002 to 2004: A case study of an unusually persistent blocking events leading to a heat wave in the Gulf of Alaska during August 2004. *Adv. Meteorol.* **2010**, 2010.

12. Jensen, A.D.; Lupo, A.R. The role of deformation and other quantities in an equation for enstrophy as applied to atmospheric blocking. *Dyn. Atmos. Oceans* **2014**, 66, 151–159.

13. Athar, H.; Lupo A.R.; Strong, C.; Dostoglou, S. A diagnostic study on atmospheric blocking using lyapunov exponents over a 50 year period. *7.12* **2007,** 7, 14-18.

14. Jensen, A.D. A Dynamic Analysis of a Record Breaking Winter Season Blocking Event. *Adv. Meteorol.* **2015**, *2015*, 634896.

15. Jensen, A.D. A dynamic analysis of a record breaking winter season blocking event. *Adv. Meteorol.* **2015,** *2015*, 634896.

16. Lupo, A.R.; Smith, P.J. Climatological features of blocking anticyclones in the Northern Hemisphere. *Tellus Ser. A* **1995**, 47, 439–456.

17. Lupo, A.R.; and P.J. Smith, Planetary and Synoptic-Scale Interactions During the Life Cycle of a Mid-Latitude Blocking Anticyclone Over the North Atlantic. *Tellus*, Special Issue: The Life Cycles of Extratropical Cyclones vol 47A, pp 575 – 596, **1995**.

18. Burkhardt, J.P.; and Lupo, A.R. The planetary and synoptic-scale interactions in a Southeast Pacific blocking episode using PV diagnostics. *J. Atmos. Sci.*, vol 62, pp 1901 – 1916, **2005**.

19. Lupo, A.R.; and Smith, P.J. The Interactions Between a Mid-Latitude Blocking Anticyclone and Synoptic-Scale Cyclones Occurring During the Northern Hemisphere Summer Season. *Mon. Wea. Rev.*, vol 126, pp 503 – 515, **1998**.

20. Lupo, A.R.; Mokhov, I.I.; Akperov, M.G.; Cherokulsky, A.V.; Athar, H. A dynamic analysis of the role of the planetary and synoptic scale in the summer of 2010 blocking episodes over the European part of Russia. *Adv. Meteorol.* **2012**, *2012*, 584257.

21. Kalnay-Rivas, E.; and Merkine, L.O. A simple mechanism for blocking. *J. Atmos. Sci.*, vol 38, pp 2077 – 2091, **1981**.

22. Mullen, S.L. Transient eddy forcing and blocking flows. *J. Atmos. Sci.*, vol. 44, pp 3 – 22, **1987**.

23. Tsou, C.H.; and Smith, P.J. The role of synoptic/planetary-scale interactions during the development of a blocking anticyclone. *Tellus*, vol 42A, pp 174 – 193, **1990**.

24. Haines, K.; and Holland, A. J. Vacillation cycles and blocking in a channel. *Quart J. Roy Meteor Soc*, vol. 124, pp 873–895, **1998**.

25. Colucci, S. J.; and Baumhefner, D. P. Numerical prediction of the onset of blocking: a case study with forecast ensembles, *Mon. Wea. Rev.*, vol 126, pp 773–784, **1998**.

26. Tilly, D. E.; Lupo, A.R.; Melick, C.J.; and Market, P.S. Calculated height tendencies in two southern hemisphere blocking and cyclone events: the contribution of diabatic heating to block intensification. *Mon. Wea. Rev.*, vol 136, pp 3568–3578, **2008**.

27. Reynolds, D.D.; Lupo, A.R.; Jensen, A.D.; Market, P.S. The predictability of Northern Hemisphere blocking using a ensemble mean forecast system. *In Proceedings of the 2nd Electronic Conference on Atmospheric Science*, Basel, Switzerland, 16–31 July **2017**.

28. Jensen, A.D.; Lupo, A.R. Using enstrophy advection as a diagnostic to identify blocking regime transition. *Q. J. R. Meteorol. Soc***. 2013.**

29. Jensen, A.D.; Lupo, A.R. Using enstrophy advection as a diagnostic to identify blocking-regime transition. *Q. J. R. Meteorol. Soc.* **2014**, 140, 1677–1683.

30. Renken, J.S.; Herman J.J.; Bradshaw, T.R.; Market, P.S.; Lupo, A.R. The Utility of the Bering Sea and East Asia Rules in Long-Range Forecasting. *Adv. Meteorol.* **2017**, *2017*, 1765428.

31. NCEP/NCAR Reanalyses Project. Available online: http://www.esrl.noaa.gov/psd/data/reanalysis/reanalysis.shtml (accessed on 3 March 2019)

32. Climate Diagnostic Bulletin. Available online: https://www.cpc.ncep.noaa.gov/products/CDB/CDB_Archive_pdf/pdf_CDB_archive.shtml (accessed on 13 March 2019)

33. Global Ensemble Forecast System (GEFS) and Northern American Ensemble Forecast System (NAEFS). Available online: https://www.emc.ncep.noaa.gov/gmb/yzhu/gif/pub/GEFSUserGuide_V1.0.pdf

34. North American Ensemble Forecast System. Available online: https://www.emc.ncep.noaa.gov/gmb/ens/NAEFS.html

35. North American Ensemble Forecast System (NAEFS). Available online: https://weather.gc.ca/ensemble/naefs/index_e.html

36. University of Missouri Blocking Archive. Available online: http://weather.missouri.edu/gcc (accessed on 14 March 2019)

37. Li, Y. 2014 The distinction of turbulence from chaos—rough dependence on initial data. *Electron. J. Differ. Equ.* **2014,** 104.

38. Eckmann, J.P.; Ruelle, D. Ergodic theory of chaos and strange attractors. *Rev. Mod. Phys.* **1985**, 57, 617-656.

39. Birk, K., Lupo, A.R., Guinan, P., Barbieri, C.E. The interannual variability of Midwestern temperatures and precipitation as related to the ENSO and PDO. *Atmósfera*. **2010,** 23:95–128.

40. Keables, M.J. Spatial variability of mid-tropospheric circulation patterns and associated surface climate in the United States during ENSO winters. *Phys Geogr*. **1992**, 13:331–348.

41. Wickens, T. D. Elementary Signal Detection Theory. *Oxford University Press.* Oxford, UK, **2001**.

42. Macmillan, N., and Creelman, C. Detection Theory: A Users Guide. *Taylor and Francis*, vol. 512, Taylor and Francis, Abingdon, UK, **2004.**

43. Tukey, J. W. Exploratory Data Analysis, AddisonWesley, *Reading MA*. **1977**, 599 pp.